**Received Date:**

**Revised Date:**

**Accepted Date:**

**Article Type: Article**

# Hepatic Sel1L-Hrd1 ER-Associated Degradation (ERAD) manages FGF21 levels and systemic metabolism via CREBH

Asmita Bhattacharya[1,2,8], Shengyi Sun[3], Heting Wang[4], Ming Liu[4,8], Qiaoming Long[5]*, Lei Yin[1,8], Sander Kersten[6], Kezhong Zhang[7], Ling Qi[1,4,8]*

[1] Department of Molecular and Integrative Physiology, University of Michigan Medical School, Ann Arbor, MI 48105, USA;

[2] Graduate Program of Genetics, Genomics and Development, Cornell University, Ithaca, NY 14853, USA;

[3] Department of Pharmacology, University of Texas Southwestern Medical Center, Dallas, TX 75390, USA

[4] Department of Endocrinology and Metabolism, Tianjin Medical University General Hospital, Tianjin 300052, China;

[5] Cam-Su Mouse Genomic Resource Center, Soochow University, Suzhou, Jiangsu 215123, China;

[6] Nutrition Metabolism and Genomics group, Wageningen University, Wageningen, The Netherlands;

[7] Center for Molecular Medicine and Genetics, Department of Immunology and Microbiology, Wayne State University School of Medicine, Detroit, MI 48201, USA;

[8] Division of Metabolism, Endocrinology & Diabetes, Department of Internal Medicine, University of Michigan Medical School, Ann Arbor, MI 48105, USA;

*** Correspondence:**

Ling Qi: lingq@med.umich.edu; Qiaoming Long: qmlong@suda.edu.cn

**Running title:** The **"**ERAD-CREBH-FGF21" axis in the liver

**Keywords:** ER quality control, Sel1L-Hrd1 ERAD, gene transcription, metabolism, FGF21

**Summary:** This study identifies Sel1L-Hrd1 ERAD as a key regulatory mechanism underlying FGF21 gene transcription via CREBH in multiple physiological settings.

**ABSTRACT**

Fibroblast growth factor 21 (Fgf21) is a liver-derived, fasting-induced hormone with broad effects on growth, nutrient metabolism and insulin sensitivity. Here, we report the discovery of a novel mechanism regulating *Fgf21* expression under growth and fasting-feeding. The Sel1L-Hrd1 complex is the most conserved branch of mammalian endoplasmic reticulum (ER)-associated degradation (ERAD) machinery. Mice with liver-specific deletion of Sel1L exhibit growth retardation with markedly elevated circulating Fgf21, reaching levels close to those in Fgf21 transgenic mice or pharmacological models. Mechanistically, we show that the Sel1L-Hrd1 ERAD complex controls *Fgf21* transcription by regulating the ubiquitination and turnover (and thus nuclear abundance) of ER-resident transcription factor Crebh, while having no effect on the other well-known Fgf21 transcription factor Pparα. Our data reveal a physiologically-regulated, inverse correlation between Sel1L-Hrd1 ERAD and Crebh-Fgf21 levels under fasting-feeding and growth. This study not only establishes the importance of Sel1L-Hrd1 ERAD in the liver in the regulation of systemic energy metabolism, but also reveals a novel hepatic "ERAD-Crebh-Fgf21" axis directly linking ER protein turnover to gene transcription and systemic metabolic regulation.

**INTRODUCTION**

The liver regulates growth and systemic energy homeostasis through inter-organ communication via the secretion of growth factors, hormones and peptides. The "starvation hormone" Fgf21 is predominantly secreted from the liver, activating energy-saving pathways that reduce activity, growth and anabolic reactions, while increasing insulin sensitivity, lipolysis and adipose tissue browning (BonDurant, Ameka et al., 2017, Fisher, Kleiner et al., 2012, Inagaki, Lin et al., 2008). Recent reports have shown the therapeutic potential of Fgf21 in a

variety of human disease conditions such as diabetes, obesity and cardiovascular disorders (Kharitonenkov & Adams, 2014, Zhao, Dunbar et al., 2012). Expression of *Fgf21* is primarily known to be induced in response to metabolic cues such as fasting by a synergistic interaction between the nuclear receptor peroxisome proliferator-activated receptor α (Pparα) and the recently identified ER-resident transcription factor cAMP-responsive element-binding protein 3-like protein 3, hepatocyte-specific (Creb3l3 or Crebh) (Badman, Pissios et al., 2007, Hondares, Rosell et al., 2010, Inagaki, Dutchak et al., 2007, Kim, Mendez et al., 2014, Omori, Imai et al., 2001). Unlike Pparα, Crebh encodes an ER membrane-anchored transcription factor, which requires regulated intramembrane proteolysis at the Golgi to generate the Crebh N-terminal fragment (Crebh-N) (Vecchi, Montosi et al., 2009, Zhang, Wang et al., 2012, Zhang, Shen et al., 2006). Subsequently, Crebh-N goes to the nucleus and is believed to recruit and form a complex with Pparα, which induces transcriptional activation of the *Fgf21* gene (Kim et al., 2014, Nakagawa, Satoh et al., 2014). While it is well known that *Fgf21* expression is induced by the nuclear receptor Pparα during fasting, how *Fgf21* expression is regulated and the importance of CREBH under physiological contexts remains to be established.

In this study, we identified a surprising link between Fgf21 gene transcription and a principal ER quality control machinery, known as ER-associated degradation (ERAD). ERAD is responsible for recognizing and retro-translocating protein substrates, misfolded or not, from the ER for cytosolic proteasomal degradation (Guerriero & Brodsky, 2012, Qi, Tsai et al., 2017). The most conserved ERAD system in mammals is the Sel1L-Hrd1 protein complex: Hrd1 being the E3 ubiquitin ligase, and Sel1L being its essential cofactor. Studies from yeast and mammalian systems have suggested that the single-spanning ER transmembrane protein Sel1L is required for the stability of Hrd1 as well as substrate recruitment and selection (Mehnert, Sommermeyer et al., 2015, Mueller, Klemm et al., 2008, Sun, Shi et al., 2014, Vashistha, Neal et al., 2016). Germline deletion of *Sel1L* or *Hrd1* in mice leads to embryonic lethality (Francisco, Singh et al., 2010, Yagishita, Ohneda et al., 2005) and acute deletion of either gene in adult mice leads to premature death (Fujita, Yagishita et al., 2015, Sun et al., 2014).

Subsequent characterization of cell type-specific Sel1L- (Ji, Kim et al., 2016, Sha, Sun et al., 2014, Shi, Somlo et al., 2017, Sun, Louri et al., 2016, Sun et al., 2014, Sun, Shi et al., 2015) and Hrd1- (Fujita et al., 2015, Kong, Yang et al., 2016, Wu, Zhao et al., 2014, Xu, Zhao et al., 2016, Yang, Qiu et al., 2014) knockout mouse models, including gene deletion in adipocytes, immune cells, enterocytes and various neurons, has revealed the significance of Sel1L-Hrd1

ERAD in a cell type- and substrate- specific manner in vivo (Qi et al., 2017). For example, mice with Sel1L deficiency in adipocytes exhibit lipodystrophy and postprandial hyperlipidemia due to the ER retention of lipoprotein lipase (LPL) (Sha et al., 2014). Further, mice with Sel1L ablation in arginine-vasopressin (AVP) neurons progressively develop polyuria and polydipsia — characteristics of diabetes insipidus, due to a maturation defect of AVP precursor, proAVP, in the ER (Shi et al., 2017). Similarly, mice with Sel1L ablation in proopiomelanocortin (POMC) neurons develop hyperphagia and obesity even under low-fat chow diet due to ER retention of POMC prohormone (Kim, Shi et al., 2018).

In the characterization of hepatocyte-specific Sel1L-deficient mice, we discovered that the Sel1L-Hrd1 ERAD complex plays a key role in regulating *Fgf21* transcription and growth in a Crebh-dependent manner. ER-resident Crebh is an unstable protein with a half-life of about 1 hour, and is targeted for proteasomal degradation by the Sel1L-Hrd1 ERAD complex. In the absence of Sel1L, Crebh accumulates intracellularly, leading to a marked elevation of *Fgf21* gene transcription in the liver and circulating Fgf21 levels. Our data further show that physiological effect of hepatic Sel1L-Hrd1 ERAD is indeed mediated, at least partially, through the CREBH-FGF21 axis. Pointing to the physiological significance of Sel1L-Hrd1 ERAD, we further showed that hepatic Sel1L-Hrd1 protein complex represses the expression of the Crebh-*Fgf21* axis during growth and fasting-feeding. Thus, this study identifies the Sel1L-Hrd1 ERAD complex as a key repressor of *Fgf21* transcription in the liver.



## RESULTS

### Expression of Sel1L-Hrd1 ERAD in the liver is responsive to physiological signals

As the liver plays a vital role in nutrient metabolism, we speculate that the levels of Sel1L-Hrd1 ERAD in the liver may fluctuate in response to metabolic signals during growth and fasting-feeding. Indeed, protein levels of hepatic Sel1L and Hrd1 were steadily elevated during growth from 3 to 24 weeks of age (Figure 1A) and were significantly higher during feeding than after an overnight fast (Figure 1B). mRNA level of Hrd1, but not Sel1L, was also elevated during growth and feeding (Appendix Figure S1A-B).

### Growth retardation of *Sel1L*$^{Alb}$ mice

To explore the role of hepatic Sel1L-Hrd1 ERAD in vivo, we generated liver-specific Sel1L knockout mice (*Sel1L*$^{Alb}$) by crossing *Sel1L*$^{f/f}$ with the hepatocyte-specific driver mouse line expressing Cre recombinase under the albumin promoter (Appendix Figure S1C). Sel1L was specifically deleted in the liver (Figure 1C), but not in other tissues such as small intestine (Appendix Figure S1D-F). The protein level of the E3 ligase Hrd1 was significantly reduced by 50% in the absence of Sel1L while its mRNA level was increased by 2.5-fold (Figure 1C and Appendix Figure S1G). On the other hand, protein levels of the previously published Sel1L-Hrd1 ERAD substrate Ire1α and Os9 (Sha et al., 2014, Sun et al., 2015) were increased by 5-10 fold in the *Sel1L*$^{Alb}$ liver (Figure 1C), while their mRNA levels were only modestly upregulated (Appendix Figure S1G).

Interestingly, both male and female *Sel1L*$^{Alb}$ mice showed significant growth retardation post weaning compared to their WT littermates on regular chow diet (Figure 1D). This growth retardation was due to shorter stature as demonstrated by body length measurements (Figure 1E-F), while ratios of organ to body weights for the liver and kidneys were unaffected (Figure 1G). Daily food intake was comparable (Figure 1H) between the two genotypes. Female *Sel1L*$^{Alb}$ mice at 2-4 months of age had reduced estrous cycle, which normally lasted 4-5 days in *Sel1L*$^{f/f}$ littermates (Figure 1I) and hence were largely infertile, but not the males.

Histological examination of the *Sel1L*$^{Alb}$ livers revealed no obvious abnormalities (Figure 1J), and there was no increase in cell death as measured by TUNEL staining (Figure EV1A) and caspase-3 cleavage (Figure 1K), nor inflammation as measured by the expression of various inflammatory genes (Figure EV1B). ER stress was only moderately increased in the Sel1L-deficient hepatocytes, as measured by Ire1α phosphorylation and *Xbp1* mRNA splicing in the livers of 9-week-old *Sel1L*$^{Alb}$ mice (Figure EV1C-D) as well as in *Sel1L*$^{Alb}$ primary hepatocytes (Figure EV1E). Morphologically, the ER in *Sel1L*$^{Alb}$ hepatocytes was dilated (Figure 1L). These observations are in line with our previous reports in several cell types such as adipocytes and enterocytes that Sel1L deficiency in vivo is associated with a mild adaptive UPR, and uncoupled from inflammation and cell death (Qi et al., 2017, Sha et al., 2014, Sun et al., 2016, Sun et al., 2014, Sun et al., 2015). Taken together, these data demonstrate that Sel1L deficiency in the liver leads to growth retardation without overt inflammation or cell death.

**Elevated Fgf21 levels in the absence of Sel1L**

To explore how deletion of Sel1L in the liver has such a profound effect on growth, we performed transcriptomics analysis of the livers from *Sel1L*$^{Alb}$ mice and their control littermates at 9-weeks of age. A total of 169 genes were significantly upregulated while 129 genes were significantly downregulated ($p < 0.05$, black dots represent fold change >2) in *Sel1L*$^{Alb}$ livers (Figure 2A). Gene set enrichment analysis confirmed significant upregulation of "protein processing in the ER", in keeping with the notion that Sel1L deficiency triggers cellular adaptation in hepatocytes. Additionally, various key metabolic pathways, including "insulin sensitivity", "PI3K-Akt pathways", "steroid hormone synthesis" and more, were significantly affected in *Sel1L*$^{Alb}$ livers (Appendix Figure S2A).

Interestingly, *Fgf21*, a fasting-induced hormone, was one of the top hits among the most highly upregulated genes in *Sel1L*$^{Alb}$ mice (Figure 2A). Quantitative PCR (qPCR) and Western blot analyses showed a 13- and 4-fold increase of *Fgf21* mRNA and protein levels, respectively, in the *Sel1L*$^{Alb}$ livers (Figure 2B-C). Strikingly, serum levels of Fgf21 were elevated by over 20-fold in *Sel1L*$^{Alb}$ mice, reaching to ~10 ng/ml vs. ~0.5 ng/ml in WT littermates (Figure 2D). As a control, *Fgf21* expression in brown and white adipose was not changed (Appendix Figure S2B).

To exclude potential developmental defects associated with chronic *Sel1L* deletion, we performed acute Sel1L deletion in the following two experiments. First, we cultured primary hepatocytes from a tamoxifen-inducible Sel1L-floxed mouse model (*Sel1L*$^{ERCre}$) and found that *Fgf21* expression was significantly increased upon the addition of tamoxifen (Figure 2E). Second, we injected 8-week-old *Sel1L*$^{f/f}$ mice once i.v. with adeno-associated virus serotype 8 (AAV8)-expressing Cre recombinase (or control GFP). Acute injection of AAV8-Cre abolished Sel1L protein level specifically in the liver, not in white adipose tissue (Figure 2F) 2-3 weeks' post injection. Similar to the chronic *Sel1L*$^{Alb}$ model, acute *Sel1L* deletion led to an 8-fold increase of hepatic *Fgf21* mRNA, and a profound 14-fold elevation of circulating Fgf21 levels (Figure 2G). Hence, these data firmly establish the key role of hepatic Sel1L-Hrd1 ERAD in regulating Fgf21 levels in both chronic and acute Sel1L-deficient models.

We next performed an unbiased comparison of genome-wide expression analyses of genes that were altered in *Sel1L*$^{Alb}$ livers to genome-wide expression analysis of genes altered in Fgf21-overexpressing transgenic mouse livers (*Fgf21 Tg*; GEO dataset series GSE39313). Indeed, the two datasets showed a large overlap among the top 15 upregulated or downregulated hepatic genes (Figure 2H and Appendix Figure S2C). This analysis further revealed a positive

correlation between the genes altered in both datasets, as evident from the polarization of the scatter plot towards the top-right and bottom-left quadrants (Figure 2I). Several examples of shared genes are highlighted in red (up-regulated) and blue (down-regulated) while those unique to each dataset, i.e. close to either axis, are marked in green (Figure 2I). Therefore, Sel1L deficiency in the liver results in elevated *Fgf21* expression and circulating Fgf21.

**Systemic metabolism changes of *Sel1L$^{Alb}$* mice are in part mediated by Fgf21**

To further establish the causal link between elevated Fgf21 levels and Sel1L-deficiency-associated systemic changes, we injected *Sel1L$^{Alb}$* mice with AAV8 encoding shRNA against *Fgf21* or control luciferase (*luc*). As a result of this knockdown, both the hepatic mRNA and circulating levels of Fgf21 in these mice were reduced by around 60% (Figure 2J-K) while having no effect on the Sel1L-Hrd1 protein levels in the liver (Appendix Figure S3A). Interestingly, this knockdown partially reversed the growth retardation (Figure 2L) and rescued the reduced female fertility (Appendix Figure S3B) of the *Sel1L$^{Alb}$* mice.

To provide further evidence for the Sel1L-Fgf21 link, we next asked whether *Sel1L$^{Alb}$* mice phenocopy Fgf21 gain-of-function models. Fgf21 has many metabolic effects aimed at promoting organismal adaptation to starvation (BonDurant et al., 2017, Potthoff, Kliewer et al., 2012). Importantly, similar to our *Sel1L$^{Alb}$* mice, Fgf21 transgenic mice also exhibited growth retardation, which was partially mediated by Stat5-dependent signaling pathways (Inagaki et al., 2008, Kharitonenkov, Shiyanova et al., 2005, Owen, Ding et al., 2014, Zhang, Xie et al., 2012). Indeed, in line with Fgf21 gain-of-function models, Stat5 phosphorylation was markedly decreased in *Sel1L$^{Alb}$* livers (Figure 3A) with diminished expression of various growth-related, p-Stat5-associated genes such as *Growth hormone receptor (Ghr), Insulin-like growth factor-1 (Igf1), Acid labile subunit (Als), $Na^+$-taurocholate cotransporting polypeptide (Ntcp), and Organic anion transporter family member-1 (Oatp1)* (Figure 3B). Moreover, in line with the suppressive effect of Fgf21 on hepatic lipogenesis (Chau, Gao et al., 2010, Zhu, Ma et al., 2014), many genes involved in hepatic lipid synthesis and transport, including *Sterol regulatory element-binding protein-1c (Srebp1c), 3-Hydroxy-3-methylglutaryl-CoA reductase (Hmgcr), Acetyl-CoA carboxylase-1/2 (Acc1/2), Low density lipoprotein receptor (Ldlr), ATP binding cassette subfamily G member-5/8 (Abcg5/8),* and *ATP binding cassette subfamily A member-1 (Abca1)* were significantly downregulated in *Sel1L$^{Alb}$* livers compared to those of their WT littermates (Figure EV2A).

In mice, Fgf21 is known to induce torpor, a hibernation-like energy-conserving, low-activity physical state (Bookout, de Groot et al., 2013, Inagaki et al., 2007). Indeed, *Sel1L*$^{Alb}$ mice exhibited lower ambulatory activity compared to that of WT littermates (Figure 3C). Moreover, similar to Fgf21 gain-of-function mouse models (Inagaki et al., 2007, Kharitonenkov et al., 2005, Owen et al., 2014), *Sel1L*$^{Alb}$ mice exhibited reduced blood glucose levels (Figure 3D), lower serum insulin levels (Figure 3E) with comparable serum glucagon levels (Figure EV2B), and significantly decreased serum triglyceride and cholesterol levels (Figure 3F-G) compared to wildtype littermates. Additionally, *Sel1L*$^{Alb}$ mice exhibited improved insulin sensitivity, but comparable glucose tolerance (Figure EV2C-D). This improved insulin sensitivity phenotype was also partially reversed upon AAV-mediated Fgf21 knockdown (Figure EV2E) in *Sel1L*$^{Alb}$ mice.

Fgf21 is known to affect white adipose tissue browning (BonDurant et al., 2017, Fisher et al., 2012, Hondares et al., 2010, Owen et al., 2014, Park, Xu et al., 2016a). Histological assessment of inguinal white adipose tissue depots from *Sel1L*$^{Alb}$ mice revealed smaller lipid droplets (Figure 3H), which was confirmed by immunostaining for the lipid droplet marker perilipin (Appendix Figure S4A-B). Indeed, in the inguinal white adipose tissues of *Sel1L*$^{Alb}$ mice, expression levels of genes associated with browning such as *Uncoupling protein-1 (Ucp1)*, and *Iodothyronine deiodinase-2 (Dio2)* were significantly elevated by ~20- and ~10-fold, respectively (Figure 3I). Protein levels of Ucp1 were tripled in inguinal white adipose tissues of *Sel1L*$^{Alb}$ mice (Figure 3J).

Fgf21 is also considered as an anti-obesity hormone owing to its ability to confer resistance to diet-induced weight gain (Kharitonenkov et al., 2005). In keeping with this, *Sel1L*$^{Alb}$ mice exhibited significantly reduced weight gain (Figure 3K) upon being fed a 60% high-fat diet, along with significantly reduced fat depots (Figure 3L and Appendix Figure S4C) and improved insulin sensitivity (Appendix Figure S4D), overall suggestive of an ameliorated response to diet-induced obesity. Therefore, we conclude that the metabolic phenotypes of *Sel1L*$^{Alb}$ mice are in part mediated through Fgf21.

**Crebh, not Pparα, accumulates intracellularly in the absence of Sel1L**

We next explored how Sel1L or Sel1L-Hrd1 ERAD is linked to *Fgf21* in the liver. *Fgf21* expression is transcriptionally controlled synergistically by nuclear receptor Pparα and Crebh. The schematic model depicting the intracellular trafficking of Crebh from ER to Golgi, proteolytic

cleavage at Golgi and nuclear entry is shown in Figure EV3A. Additionally, Fgf21 expression may also be regulated via transcription factors such as Xbp1s in response to ER stress (De Sousa-Coelho, Marrero et al., 2012, De Sousa-Coelho, Relat et al., 2013, Kim, Kim et al., 2013b, Laeger, Henagan et al., 2014, Wan, Lu et al., 2014); however, the physiological significance of these regulators remains to be established.

Excitingly, Crebh protein levels were significantly elevated (> 20-fold) in the livers of *Sel1L*$^{Alb}$ mice at 9-weeks of age (Figure 4A and quantitated in Figure 4C). By contrast, the protein levels of Pparα and Xbp1s were unchanged (Figure 4B and quantitated in Figure 4C). Importantly, this Crebh protein accumulation was due to a post-transcriptional mechanism as the mRNA levels of *Crebh* were not affected by Sel1L deficiency (Figure 4D). Moreover, the nuclear, active form of Crebh (Crebh-N) was also significantly upregulated by ~8 fold in *Sel1L*$^{Alb}$ livers (Figure 4B and quantitated in Figure 4C). Similar induction of Crebh protein was observed in the livers of adult mice with acute deletion of Sel1L (Figure 4E).

Q-PCR analysis further confirmed that, in addition to *Fgf21*, several other known Crebh target genes, such as *Amyloid P component, serum (Apcs), Apolipoprotein-A4 (Apoa4),* and *Cell death inducing DFFA like effector c (Cidec)* (Park et al., 2016a, Park, Xu et al., 2016b, Xu, Park et al., 2014, Zhang et al., 2006), were also significantly upregulated in *Sel1L*$^{Alb}$ livers (Figure EV3B). In contrast, canonical Pparα targets such as *Acyl-CoA synthetase long-chain family member 1 (Acsl1), Carnitine palmitoyltransferase 1A (Cpt1a), Acyl-CoA oxidase 1, (Acox1)* and *Microsomal triglyceride transfer protein (Mttp)* were significantly downregulated in *Sel1L*$^{Alb}$ livers (Figure EV3C).

As *Fgf21* expression is reportedly induced by ER stress (Jiang, Yan et al., 2014, Kim, Jeong et al., 2013a, Schaap, Kremer et al., 2013), we next compared the effect of Sel1L-Hrd1 ERAD deficiency to pharmacological UPR activation on Crebh accumulation and *Fgf21* expression. First, the Crebh protein accumulation in *Sel1L*$^{Alb}$ livers was much higher than that in the livers of wildtype mice challenged with the potent pharmacological ER stress inducer tunicamycin (Figure 4F). Additionally, the transcriptional induction of *Fgf21* in *Sel1L*$^{Alb}$ livers or primary hepatocytes was much more pronounced compared to that in tunicamycin-challenged WT liver or in thapsigargin-treated WT primary hepatocytes (Figure EV3D-E), in spite of much higher ER stress observed in the latter (Figure EV1C-E). We conclude that hepatic Sel1L-Hrd1 ERAD

regulates *Fgf21* induction through a mechanism involving Crebh, but independently of Pparα- or ER stress.

Like the other recently characterized Sel1L-Hrd1 ERAD substrate Ire1α (Sun et al., 2015), the accumulated Crebh protein in Sel1L-deficient hepatocytes remained soluble in mild detergent NP40 (Figure 4G), suggesting that Crebh does not form insoluble aggregates in the absence of Sel1L-Hrd1 ERAD. Moreover, confocal immunostaining of Crebh further demonstrated the intracellular accumulation of Crebh protein including in the nucleus of *Sel1L*$^{Alb}$ hepatocytes when compared to WT livers (Figure 4H and zoomed-out images shown in Figure EV3F). Chromatin immunoprecipitation (ChIP) of Crebh revealed increased binding of Crebh onto the proximal promoter of the *Fgf21* gene in *Sel1L*$^{Alb}$ liver versus WT liver (Figure 4I).

Finally, to demonstrate a similar mechanism in human hepatocytes, we knocked out Sel1L via the CRISPR/Cas9 system in the human hepatoma cell line Hep3B. Acute deletion of Sel1L significantly increased CREBH protein level and *Fgf21* gene expression (Figure 4J-K). Taken together, we conclude that Sel1L deficiency in the liver leads to intracellular and nuclear accumulation of Crebh in both mice and humans.

**ER-resident Crebh is an endogenous Sel1L-Hrd1 ERAD substrate**

A marked accumulation of Crebh protein in Sel1L-deficient cells prompted us to test the hypothesis that Crebh is a bona fide endogenous Sel1L-Hrd1 ERAD substrate in the liver. In keeping with our hypothesis, a previous study showed that Crebh is degraded by proteasomes (Bailey, Barreca et al., 2007), but the nature and significance of this degradation event remains unknown. Indeed, Crebh protein was unstable with a half-life of about 45 minutes in Crebh-transfected HEK293T cells treated with the translation inhibitor cycloheximide (Figure 5A). Crebh protein became greatly stabilized with half-lives of over 4 hours in *SEL1L-/-* and *HRD1-/-* cells (Figure 5A and Figure EV4A). Notably, accumulation and stabilization of Crebh protein were more pronounced in *HRD1-/-* cells than in *SEL1L-/-* cells, potentially owing to the residual Hrd1 protein in SEL1L-/- cells (Figure 1C) (Kim et al., 2018).

As Crebh is cleaved in the Golgi to generate N-terminal fragment Crebh-N, we next generate cleavage-defective-Crebh by mutating its S1P and S2P cleavage sites (Zhang et al., 2006). Indeed, similar to wildtype Crebh, non-cleavable Crebh mutant was unstable and became stabilized in the absence of Sel1L and Hrd1 (Figure EV4B). Moreover, unlike Crebh, steady-

state protein levels and half-life of Crebh-N protein were not affected by Hrd1 deficiency (Figure EV4C-D). Hence, these data point to the specificity of the Sel1L-Hrd1 ERAD effect towards ER-resident Crebh, not cleaved the Crebh-N fragment.

To further examine the contribution of proteasomes versus lysosomes in the clearance of Crebh protein, we treated Crebh-transfected cells with proteasome inhibitor bortezomib (BTZ) or lysosomal inhibitor chloroquine (CHQ) in the presence of cycloheximide (CHX). BTZ, but not CHQ, stabilized Crebh protein (Figure 5B). Moreover, the effect of BTZ on Crebh protein was dampened in HRD1-deficient cells (Figure 5C), further supporting the notion that degradation of Crebh is largely mediated by the Sel1L-Hrd1 ERAD complex.

Crebh interacted strongly with both Hrd1 and Sel1L under regular native immunoprecipitation conditions (Figure EV4E-F and Lane 2, Figure 5D). Additionally, following lysate denaturing prior to immunoprecipitation, robust ubiquitination of Crebh protein was detected and blocked upon expression of catalytically inactive Hrd1 C2A mutant (top panel Lanes 1-3, Figure 5D). In contrast, Crebh-N did not interact strongly with, nor was ubiquitinated by, Hrd1 (Lanes 4-5, Figure 5D). Together, these data demonstrate that Crebh is targeted for proteasomal degradation by Sel1L-Hrd1 ERAD, requiring the activity of Hrd1 E3 ligase.

**Sel1L-Hrd1 ERAD deficiency does not affect the ER-to-Golgi trafficking of Crebh**

Although ER stress was previously reported to be required for the ER exit of Crebh (Zhang et al., 2006), a recent study suggested that may not be the case, but rather Crebh constitutively migrates to the Golgi (Xu et al., 2014). Does Sel1L-Hrd1 ERAD affect ER-to-Golgi trafficking of Crebh? As Crebh undergoes N-linked glycosylation in the ER, a step required for its ER exit to Golgi (Bailey et al., 2007, Chan, Mak et al., 2010), we next tested the endoglycosidase-H (endoH) sensitivity of Crebh protein to distinguish ER- versus Golgi-resident Crebh. Interestingly, despite having elevated total protein level at the basal state, Sel1L-deficient liver exhibited a similar percent of endoH resistant to sensitive Crebh protein to that in WT liver (Lanes 3 vs. 4, Figure 5E). Indeed, at the steady state, nearly 50% of CREBH were endoH resistant, i.e. at the Golgi, regardless of ERAD status, suggesting that a large portion of CREBH constitutively exits the ER. As a control, Sel1L as an ER-resident protein was completely endoH sensitive (Lanes 1 vs. 3, Figure 5E). Hence, our data suggest that Sel1L-Hrd1 ERAD does not regulate the trafficking of Crebh from the ER to Golgi.

**Crebh links hepatic Sel1L-Hrd1 ERAD to Fgf21 and systemic metabolic regulation**

To demonstrate whether Crebh indeed links Sel1L-Hrd1 ERAD to Fgf21 and systemic metabolic regulation, we deleted Crebh in the livers of *Sel1L*$^{Alb}$ mice by i.v. injecting GFP-encoding AAV8 expressing shRNA against *Crebh* (*shCrebh*) or control luciferase (*shLuc*). Five weeks after AAV injection, GFP-positive livers were observed in all cohorts (Figure EV5A). *shCrebh* injection resulted in a ~60% reduction of Crebh protein and mRNA levels in *Sel1L*$^{Alb}$ livers (Figure 6A-B), and in conjunction, both mRNA and circulating levels of Fgf21 in *Sel1L*$^{Alb}$ mice were reduced by ~75% (Figure 6B-C). Importantly, the ER stress response markers such as *Xbp1* mRNA splicing and Ire1a/Perk pathway activation was not affected by Crebh knockdown in *shCrebh*-injected *Sel1L*$^{Alb}$ livers compared to the *shLuc*-injected *Sel1L*$^{Alb}$ livers (Figure EV5B-D), further underscoring that the effect of Sel1L-Hrd1 ERAD on Fgf21 is largely uncoupled from ER stress.

Upon Crebh deletion, the expression levels of p-Stat5-depdendent, growth-associated genes were also elevated in *Sel1L*$^{Alb}$ mice compared to those receiving *shLuc* (Figure 6D). Indeed, *Sel1L*$^{Alb}$ mice with Crebh deletion showed better weight gain than *Sel1L*$^{Alb}$ mice injected with *shLuc* control (Figure 6E and Figure EV5E). Moreover, deletion of Crebh in *Sel1L*$^{Alb}$ mice also partially reversed the insulin sensitivity of *Sel1L*$^{Alb}$ mice (Figure 6F). Lastly, Crebh knockdown markedly reduced the Ucp1 expression in white adipose tissue that was observed in *Sel1L*$^{Alb}$ mice (Figure 6G-H). Hence, hepatic Sel1L-Hrd1 ERAD regulates growth and systemic metabolism, at least in part, via the suppression of the "Crebh-Fgf21" axis.

**Sel1L-Hrd1 ERAD suppresses "Crebh-Fgf21" axis under multiple physiological contexts**

The above results pointed to Sel1L-Hrd1 ERAD as a key regulator of the "Crebh-Fgf21" axis with significant impact on systemic metabolism. We next asked whether there is a correlation between Sel1L-Hrd1 ERAD and Crebh-Fgf21 under two physiological settings – fasting-feeding and growth.

During feeding, hepatic Sel1L and Hrd1 levels were markedly higher than during fasting (Figure 1B and Lanes 3 vs. 4, Figure 7A), while protein levels of Crebh and Crebh-N exhibited the opposite trend (Lanes 3 vs. 4 and 1 vs. 2, Figure 7A). Indeed, there was negative correlation between Sel1L-Hrd1 proteins and Crebh protein/*Fgf21* mRNA levels under fasting-feeding (Figure 7B). Furthermore, Crebh protein level was highly elevated and remained largely constant during fasting-feeding in Sel1L-deficient liver (Lanes 7-8 vs. 3-4, Figure 7A and quantitated in Figure 7C), suggesting that Sel1L-Hrd1 ERAD is largely responsible for the

decline of Crebh protein level in the fed state. Consequently, the circulating levels of Fgf21 were also greatly elevated in both fasted and fed states of Sel1L-deficient mice (Figure 7D).

During growth, hepatic Sel1L and Hrd1 proteins also steadily increased with age from 3 to 24 weeks (Figure 1A and Lanes 4-6, Figure 7E), while protein levels of both Crebh and Crebh-N steadily decreased (Lanes 1-6, Figure 7E). There was a negative correlation between Sel1L-Hrd1 proteins and Crebh protein/*Fgf21* mRNA levels in WT mice during growth (Figure 7F). Importantly, in the *Sel1L*$^{Alb}$ mice, the decline of hepatic Crebh protein were markedly blunted by the Sel1L deficiency (Lanes 7-12 vs. 1-6, Figure 7E and quantitated in Figure 7G). This results in highly elevated circulating Fgf21 levels over the different ages of the *Sel1L*$^{Alb}$ mice, unlike the gradual decline with age in WT mice (Figure 7H).

Therefore, these data not only demonstrate an inverse association between hepatic Sel1L-Hrd1 ERAD and Crebh protein levels under various physiological setting, but also establish Sel1L-Hrd1 ERAD as a key repressor of the "Crebh-Fgf21" axis during growth and fasting-feeding.



**DISCUSSION**

The liver controls overall energy metabolism and regulates a wide range of key processes in the body, including growth and fasting-feeding cycle (Lajtha, Latzkovits et al., 1976). The hepatokine Fgf21 is a key metabolic endocrine hormone involved in inter-organ crosstalk and is considered as a potent therapeutic agent for the treatment of obesity and obesity-associated diabetes (Fisher & Maratos-Flier, 2016). This study reports Sel1L-Hrd1 ERAD as a key physiological repressor of Fgf21 gene transcription in the nucleus under various metabolic states in the body. Indeed, our data reveal a common mechanism by which diverse physiological contexts such as fasting-feeding and growth integrate at the level of Sel1L-Hrd1 ERAD via the control of Crebh protein abundance on the ER membrane to regulate *Fgf21* gene transcription (Figure 8). This metabolic tuning of Fgf21 levels by Sel1L-Hrd1 ERAD plays a key role in setting the normal growth and physiological paradigm in the body, as evident from the strong metabolic phenotypes of *Sel1L*$^{Alb}$ mice.

Our study reveals that growth and feeding can both increase the expression of the Sel1L-Hrd1 ERAD protein complex in the ER, which in turn negatively regulates the protein level of Crebh and Fgf21 gene transcription. ER-resident Crebh protein is unstable and its abundance is tightly controlled by the Sel1L-Hrd1 protein complex. Indeed, Crebh or Fgf21 deletion in Sel1L-deficient mice significantly reverses or attenuates some growth and metabolic phenotypes of the hepatic Sel1L-deficient mice, suggesting that hepatic Sel1L-Hrd1 ERAD effect is at least partially mediated through the "Crebh-Fgf21" axis. The impact of Sel1L-Hrd1 ERAD deficiency on Crebh and *Fgf21* induction is profound, as demonstrated by the dramatic elevation of serum Fgf21 levels (~10 ng/ml), nearly reaching those in models of transgenic Fgf21-overexpression or pharmacological administration (~10-25 ng/ml). Therefore, systemic energy homeostasis and *Fgf21* expression, both in the liver and circulation, is tightly linked to the activity of hepatic Sel1L-Hrd1 ERAD, the expression of which, in turn, may be responsive to the metabolic state of the body. For example, specific hormones and metabolites (such as insulin, glucagon, leptin, corticosterone, glucose, fatty acids etc.) associated with fasting-feeding and/or growth may be involved in the transcriptional regulation of Sel1L and/or Hrd1. In this regard, further investigation will be needed to dissect the molecular pathways that link physiological cues to hepatic ERAD gene expression.

An outstanding question remains as to which transcription factor – Crebh or Pparα – is the more pertinent regulator of *Fgf21* expression in the liver in response to physiological cues. A recent study showed that Crebh is required for transcriptional activation of *Fgf21* by Pparα by forming the Crebh-Pparα complex and also by regulating the expression of *Pparα* (Kim et al., 2014). Our study demonstrates a profound effect of Sel1L-Hrd1 ERAD on *Fgf21* gene transcription via Crebh, but not Pparα, during growth and fasting-feeding. Although our study does not exclude the importance of Pparα in *Fgf21* transcription, it reveals another layer of regulation of *Fgf21* expression during fasting-feeding and growth, centered at the level of ER membrane.

ERAD is often considered to be responsible for clearing "misfolded" proteins from the ER, and hence ERAD deficiency is mostly known to cause the accumulation of misfolded proteins and thereby trigger ER stress. Indeed, one recurrent question associated with ERAD-deficient models is whether the presumptive induction of ER stress in ERAD deficiency is the true cause of observed phenotypes. Our data show that the effect of ER stress on Crebh and *Fgf21* expression pales when compared to that of Sel1L-Hrd1 ERAD deficiency in the liver or hepatocytes. Moreover, our data showed that Sel1L deficiency only triggers very moderate ER

stress response, likely due to cellular adaptation as shown in other cell types (Kim et al., 2018, Shi et al., 2017). Hence, while modest but tonic ER stress may contribute somewhat to the overall phenotype of the Sel1L-deficient mice, the marked elevation of Fgf21 is likely a direct result of Crebh stabilization and accumulation in the absence of Sel1L-Hrd1 ERAD. Indeed, a recent study reported that ER stress is dispensable for Crebh activation in the liver (Xu et al., 2014). Providing further support to our model, none of the previous hepatic UPR mouse models showed metabolic phenotypes similar to our hepatocyte-specific Sel1L-Hrd1 ERAD-deficient system or to the Fgf21 gain-of-function mouse models (Hur, So et al., 2012, Jurczak, Lee et al., 2012, Lee, Scapa et al., 2008, Olivares & Henkel, 2015, So, Hur et al., 2012, Zhang, Wang et al., 2011). For example, genetic ablation of the UPR sensor Ire1α alters lipid metabolism and ketogenic programs in the liver (So et al., 2012, Zhang et al., 2011). Silencing a major Ire1α effector *X-box Binding Protein-1 (Xbp1)* in the liver leads to marked disequilibrium in lipid homeostasis and impaired recovery from pharmacologically induced ER stress (Olivares & Henkel, 2015). Thus, we believe that mammalian Sel1L-Hrd1 ERAD in the liver plays an intimate and critical role in growth and fasting-feeding by directly regulating the activity of the "Crebh-Fgf21" axis. Additionally, liver specific deletion of *Autophagy related-7 (Atg7)* appears to lead to improved energy metabolism in the body owing to mitochondrial defect-associated Fgf21 production (Kim et al., 2013a). While we did not find any mitochondrial structural defects in our Sel1L-deficient livers, further investigation will be done to assess the relative importance and potential crosstalk between these two, distinct cellular quality control pathways in modulating Fgf21 expression under physiological contexts.

Overall, this study delineates a novel role of Sel1L-Hrd1 ERAD in the liver, and importantly, establishes Sel1L-Hrd1 ERAD-mediated Crebh degradation as an important regulatory mechanism underlying *Fgf21* transcription regulation. This novel "ERAD-Crebh-Fgf21" cascade from the ER to the nucleus (Figure 8) represents another beautiful example of the regulation of cellular, and in this case, systemic response by Sel1L-Hrd1 ERAD and may provide with multiple components that could be utilized for therapeutic intervention in diseases associated with growth defects, lipid disequilibrium and insulin resistance.



## MATERIALS AND METHODS

**Mice**. The *Sel1L*$^{f/f}$ mice (Sun et al., 2014) were crossed with mice expressing Albumin-promoter-driven Cre on the C57BL/6J background (JAX 003574, B6.Cg-Tg(Alb-Cre)21Mgn/J) to generate hepatocyte-specific Sel1L deficient mice (*Sel1L*$^{Alb}$) and its WT littermates *Sel1L*$^{f/f}$. Due to the infertility of *Sel1L*$^{Alb}$ female mice, only male *Sel1L*$^{Alb}$ mice were used for breeding. Mice were fed a low-fat diet (13% fat, 57% carbohydrate, and 30% protein, LabDiet 5LOD) or a high-fat diet (60% fat, 20% carbohydrate, and 20% protein) where indicated. Comprehensive Lab Animal Monitoring System (CLAMS, Columbus Instruments) was used with 1 day acclimatization period followed by 1 day measurement for metabolic cage analyses studies. Mice were housed on a regular 12-hour light/dark cycle and regulated temperature (22℃). All animal procedures were done in accordance with the IACUC at Cornell University (2007-0051) and University of Michigan Medical School (PRO00006888). Mice were routinely fasted in the morning for 5-6 hours before sacrifice except as whenever stated (e.g. longer fasting or ad libitum). Mice were fasted for 6 hours before ITT and 16 hours overnight before GTT experiments. Cervical dislocation was used for euthanasia and tissues were immediately either fixed or frozen in liquid nitrogen upon collection. Vaginal smears were examined on a daily basis for estrus cycle analysis.

Based on sample size formula of power analysis, 4-6 mice per group is the minimal number of animals to obtain statistical significance. A total of 4-10 mice was routinely used in each study to ensure adequate power. No samples or animals were excluded from analyses. Mice in each group were randomly chosen for experiment, matching in age, genotype and gender. The investigators were not blinded during experiments and result assessment.

**Serum metabolite analysis**. Multiplex analysis was carried out with appropriate standards and blanks for serum insulin and glucagon measurement. Serum triglycerides (TG) and cholesterol (CHOL) was measured by IDEXX Laboratories. Blood glucose was measured via the TrueTest Glucometer. Serum levels of Fgf21 was measured by ELISA analyses as per the protocol provided by the mouse Fgf21 ELISA kit (R&D Systems MF2100).

**Western blot analysis**. Protein extraction from cell and tissue lysates and Western blotting following SDS-PAGE separation (and phos-tag gel for p-Ire1α) were performed as previously described (Qi, Yang et al., 2011, Sha, He et al., 2009, Yang, Xue et al., 2010). The quantification of signals was done using BioRad ImageLab software and protein levels among samples were normalized to Hsp90, β-actin or α-tubulin as loading controls. The commercially

available antibodies used are as follows: Flag (1:500 for staining, 1:5000 for Western blot; Sigma F1804); HA (1:3,000; Sigma H9658); Myc (1:1000; Sigma); Ucp1 (1:10,000; Sigma U6382); Hsp90 (1:4,000; Santa Cruz sc-7947); α-tubulin (1:2,000; Santa Cruz sc-5286); lamin (1:1000; Santa Cruz sc-6215); Xbp1 (1:1000; Santa Cruz sc-7160); BiP (1:1,000; Santa Cruz sc-1051); KDEL (1:500; Abcam ab50601); Sel1L (1:2,000; Abcam ab78298); Os9 (1:5,000; Abcam ab109510); β-actin (1:10,000, Abcam ab20272); Crebh (1:1000 for Western, 1:100 for immunostaining; Kerafast EWS101); Fgf21 (1:1000; R&D AF3057); Pparα (1:500; Millipore MAB3890); Perilipin (1:200; Cell Signaling 9349); phospho-Stat5 (1:1000; Cell Signaling 9359); Stat5 (1:1000; Cell Signaling #94205); Ire1α (1:2,000; Cell Signaling 3294); Perk (1:1,000; Cell Signaling 3192); p-eIf2α (1:1,000; Cell Signaling 9721); eIF2α (1:2,000; Cell Signaling 9722); caspase-3 (1:1,000; Cell Signaling 9665); cleaved-caspase-3 (1:1,000; Cell Signaling 9661). Hrd1 antibody (1:300) was kindly provided by Dr. Richard Wojcikiewicz (SUNY Upstate Medical University); H2a antibody (1:5,000) was kindly provided by Dr. Yihong Ye (NIDDK). Secondary antibodies for Western blot were goat anti-rabbit IgG-HRP and goat anti-mouse IgG-HRP (1:5,000; BioRad), and donkey anti-goat IgG-HRP (1:5000; Jackson ImmunoResearch). Secondary antibodies for immunostaining were anti-mouse IgG Cy3 and FITC; anti-rabbit IgG Alexa Fluor 488, Alexa Fluor 594, Alexa Fluor 647; and anti-goat IgG Alexa Fluor 594, Alexa Fluor 680 (all 1:500; Jackson ImmunoResearch).

**Immunoprecipitation.** Cells/tissue were lysed in a buffer containing 150 mM NaCl, 50 mM Tris-HCl pH 7.5, 1 mM EDTA, 1% NP-40, protease inhibitors and phosphatase inhibitors, and 10 mM N-ethylmaleimide. A total of 2-6 mg protein lysates was incubated with antibody coated agarose beads overnight with gentle rocking at 4℃. Immuno-complexes were washed in a buffer containing 137 mM NaCl, 20 mM Tris-HCl pH 7.5, 2 mM EDTA and 10% glycerol and eluted by boiling at 95℃ for 5 mins in SDS sample buffer. For “denaturing” immunoprecipitation conditions in Figure 5D, lysis was first carried out in 200 µl of above stated buffer with 5 mM DTT and 1% SDS, and denatured for 10 min at 95℃ before diluting 1:5 with lysis buffer and continuing with antibody incubation.

**Detergent solubility analysis.** Frozen liver tissue was weighed and homogenized as previously described in NP40 lysis buffer. The lysate volume was then normalized by tissue weight and protein concentration via Bradford assay. The lysate was then centrifuged for 10 minutes at 12,000g and the supernatant collected was the NP40-Soluble fraction after addition of 5X SDS-containing sample buffer and heating at 65℃ for 15 minutes. The pellet obtained

was re-suspended in 1X SDS sample buffer with a volume normalized to its corresponding soluble fraction, and boiled at 95℃ for 30 minutes to form the NP40-Insoluble/Pellet fraction.

**Nuclear fractionation**. Nuclear fractionation of the liver was performed as previously described (Sha et al., 2009).

**RNA extraction, RT and qPCR**. Total RNA was extracted from liver tissues and cells using Trizol and BCP phase separation reagent, and RNA quality was measured via OD. RT–PCR for Xbp1 splicing was performed as previously described (Sha et al., 2009). qPCR analysis was carried out using Taq polymerase, oilgo-dT primer, SYBR-Green based master mix and Applied Biosystems qPCR machine. All PCR data were normalized to the ribosomal *L32* gene expression level. qPCR primer sequences are: *Sel1L* F: TGGGTTTTCTCTCTCTCCTCTG, R: CCTTTGTTCCGGTTACTTCTTG; *Hrd1* F: AGCTACTTCAGTGAACCCCACT, R: CTCCTCTACAATGCCCACTGAC; *Os9* F: GCTGGCTGACTGATGAGGAT, R: CGGTAGTTGCTCTCCAGCTC; *Ire1α* F: CTGTGGTCAAGATGGACTGG, R: GAAGCGGGAAGTGAAGTAGC; *BiP* F: TGTGGTACCCACCAAGAAGTC, R: TTCAGCTGTCACTCGGAGAAT; *Chop* F: TATCTCATCCCCAGGAAACG, R: GGGCACTGACCACTCTGTTT; *Fgf21* F: CTGGGGGTCTACCAAGCATA, R: CACCCAGGATTTGAATGACC; *Ghr* F: AGCCTCGATTCACAAGTGTCG, R: GATGACCAATTCTTGCAGCTTG; *Igf1* F: GCTCTTCAGTTCGTGTGTGGAC, R: TTGGGCTGTCAGTGTGGCGC; *Als* F: AACCTCAGGAATAACTCCTTGC, R: CACCGGCTGGCAGTCATCTCCC; *Oatp1* F: CCTCAGCTGTACAATGATTGCC, R: TTTTGGTTCAATGCAGGGTTG; *Ntcp* F: GAAGTCCAAAAGGCCACACTATGT, R: ACAGCCACAGAGAGGGAGAAAG; *Abcg5* F: TCAATGAGTTTTACGGCCTGAA, R: GCACATCGGGTGATTTAGCA; *Abcg8* F: TGCCCACCTTCCACATGTC, R: ATGAAGCCGGCAGTAAGGTAGA; *Ldlr* F: AGGCTGTGGGCTCCATAGG, R: TGCGGTCCAGGGTCATCT; *Hmgcr* F: CTTGTGGAATGCCTTGTGATTG, R: AGCCGAAGCAGCACATGAT; *Srebp1c* F: GGAGCCATGGATTGCACATT, R: CCTGTCTCACCCCCAGCATA; *Abca1* F: GCTTGTTGGCCTCAGTTAAGG, R: GTAGCTCAGGCGTACAGAGAT; *Crebh* F: CAGCTCAAGAAAGCAGGAAG, R: AGCTGCTCCAGAAGAGACAA; *Ppara* F: GCGTACGGCAATGGCTTTAT, R: GAACGGCTTCCTCAGGTTCTT; *Ucp1* F: CCAGTGGATGTGGTAAAAACAA, R: TCAAAGCACACAAACATGATGA; *Dio2* F: CAGTGTGGTGCACGTCTCCAATC, R: TGAACCAAAGTTGACCACCAG; *Cidea* F: TGCTCTTCTGTATCGCCCAGT, R:

GCCGTGTTAAGGAATCTGCTG; *Apcs* F: ACAGTCCGTGGTATGGAAGA, R: TGGGGCTTTCACAGTGTATT; *Apoa4* F: CCAGCTAAGCAACAATGCCA, R: TGGAAGAGGGTACTGAGCTGC; *Cidec* F: ATGGACTACGCCATGAAGTCT, R: CGGTGCTAACACGACAGGG; *Acc1* F: ATGGGCGGAATGGTCTCTTTC, R: TGGGGACCTTGTCTTCATCAT; *Acc2* F: CACCATCCGTGAAAACATCA, R: AGCAGCTGAGCCACCTGTAT; *Xbp1* F: ACACGCTTGGGAATGGACAC, R: CCATGGGAAGATGTTCTGGG; *Acsl1*: F: AACGATGTACGATGGCTTCC, R: CATATGGCTGGTTTGGCTTT; *Acox1*: F: GATGTGACCCTTGGCTCTGT, R: AGAGATTCGGCCTCTCTGTG; *Cpt1a* F: ATGACGGCTATGGTGTTTCC, R: GGCTTGTCTCAAGTGCTTCC; *Mttp*: F: TACCCGTTCTTGGTCTGCAT, R: TCTGGCTGAGGTGGGAATAC.

**Primary hepatocyte culture**. Mice (6-8 weeks of age) were euthanized with isoflurane inhalation, and the liver was perfused first with warm calcium/magnesium-free HBSS containing 25 mM HEPES, EDTA, 1% penicillin-streptomycin, and then with warm calcium/magnesium-free HBSS containing 25 mM HEPES, 2 mM CaCl2, 1% penicillin-streptomycin and 0.75 mg/ml collagenase (Sigma-Aldrich C8051). After removal and mechanical dispersion of the swollen, digested liver, cells were suspended in ice-cold plating medium (DMEM with 2% Sodium pyruvate, 2% penicillin-streptomycin, 10% heat-inactivated FBS, 1 μM dexamethasone and 0.1 μM insulin) and passed through a 70 μm cell strainer. The cells were then pelleted by centrifugation for 3 min at 60×g at 11℃ and re-suspended buffered Percoll before pelleting by centrifugation for 4 min at 800×g at 11℃. The final cells were washed thrice in plating medium (centrifugation for 3 min at 60×g at 11℃), viability-checked (via trypan blue exclusion as >80%), and plated on 6-well plates. Once the cells attached well (2-4 hours after plating), the plating medium was replaced with culture medium (DMEM containing 2% Sodium pyruvate, 2% penicillin-streptomycin, 0.2% BSA, 0.1uM dexamethasone and 1nM insulin). Before treatment with nutrients/hormones, the cells were kept in starvation media (no serum/growth factors/hormones) for 4 hours.

**Chromatin Immunoprecipitation**. Chromatin IP from liver tissue was carried out as per the protocol previously described (Murgatroyd, Hoffmann et al., 2012) using 1:250-500 dilution of the Crebh antibody, regular Protein A agarose beads (Invitrogen) instead of magnetic beads, and phenol-chloroform-based DNA extraction in place of columns. The final precipitated DNA was amplified via qPCR using following primers: *Fgf21* promoter (positions -8 to -125 relative to

transcribed region) F: ATCCCCAGCTGAGAAGACAC, R: GCCCTTTTCATTCAGACCCC; end of *Fgf21* coding sequence (positions +1214 to +1439 relative to transcribed region) F: AAGGCTCTACCATGCTCAGG, R: CGTCTGCCTCAGAAGGACTC.

**Immunostaining and histology**. For H&E staining, tissues upon dissection were directly placed in 10% neutral buffered formalin, stored at 4℃, and processed by the Michigan Histology Core for paraffin embedding, section cutting and H&E staining on a fee-for-service basis. For other in vivo staining, livers on anesthetized mice were perfused first with PBS and then with 4% paraformaldehyde for fixation. After further overnight fixation, the tissues were dehydrated overnight in 15% sucrose solution and then frozen in Tissue-Tek O.C.T. Compound. 5 µm sections were cut using a cryotome for further staining. During immunocytochemistry, cells were cultured on poly-L-lysine coated coverslips and were fixed in 4% formalin for 10 mins. For paraffin embedded sections, boiling in 1mM EDTA for 25 minutes was done for antigen retrieval. For cryo-sections and cells, permeabilization was carried out in 0.3% Triton X-100 and 0.3% Glycine for 10 min at room temperature. Thereafter, the sections/cells and incubated in blocking solution (1% donkey serum, 0.03% TritonX-100 in PBS) for 40-60 minutes at room temperature, and then incubated with primary antibodies for 24-72 hours, as needed at 4℃ in humidified chambers. Thereafter, they were washed thrice with PBST (0.03% TritonX-100 in PBS) and incubated with secondary antibodies for 2 hours at room temperature. Counterstaining and mounting were performed using hard-set mounting medium containing DAPI (Vector H-1200). Fluorescent samples were imaged with Nikon A1 Confocal Microscope at the University of Michigan Imaging Core using identical imaging parameters within each experiment. H&E stained samples were scanned using Aperio Scanscope (Leica Biosystems). Images were processed using ImageJ plugin (FIJI).

**TUNEL assay**. Paraffin embedded liver sections were subjected to TUNEL assay as per manufacturer's protocol using the In-Situ Cell Death detection kit (Roche, 11684795910). Images were obtained by Zeiss LSM710 Confocal Microscope at the Cornell University Biotechnology Resource Center Imaging Facility.

**Transmission Electron Microscopy (TEM)**. The livers of anesthetized mice were perfused via the hepatic portal vein first with Sorenson's buffer to wash out the blood and then with 2.5% glutaraldehyde and 4% paraformaldehyde in 0.1M Na-cacodylate buffer as fixative. The liver was then cut into tiny pieces (about 1-2mm cubes) and soaked overnight in the same fixative.

Thereafter, the samples were submitted to the University of Michigan Histology and Imaging Core for washing, embedding, sectioning and imaging via TEM.

**Cell lines and transfection**. Cells lines were cultured in DMEM (Corning, NY) containing 1% penicillin/streptomycin, 1% sodium pyruvate and heat inactivated 10% FBS (GIBCO). Cells were transfected within 16-22 hours after plating with Lipofectamine 2000 and harvested around 24 hours after. Human hepatoma Hep3B cells were used to generate CRISPR knockouts of SEL1L via lentiviral packaging system with guide sequences ACTGCAGGCAGAGTAGTTGC and GACATCAGATGAGTCAGTAA. *HRD1-/-* HEK293T cells were previously described (Shi et al., 2017), and *Sel1L-/-* and *Hrd1-/-* N2a cells were previously described (Kim et al., 2018). An attempt to overexpress Sel1L in cells resulted in complications in cell survival, an issue currently under further investigation.

**Plasmids**. All Crebh plasmid constructs (Crebh, Crebh-N) were generated as described (Zhang et al., 2006). The pAAV8-D(+)-U6-siRNA-CMV-GFP vector was purchased from Addgene. Myc-tagged WT and mutant (C2A) Hrd1 constructs were kindly provided by Dr. Yihong Ye (NIDDK). pcDNA3-HA-Ub was a kind gift from Dr. Hideki Nishitoh (University of Miyazaki, Japan). Sequences used for mutagenesis to generate cleavage defective Crebh (mutating to Alanines the RNNNRNL of the S1P cleavage site to ANNNANA and the LP of the S2P cleavage site to AA) is as follows, with the new Alanines underlined:
CCTCATCATCGCCGCCTCCATCAGCCCTTTTGGCCCCAACAAAACCGAGAGCCCTGGGGA
CTTTGCGCCTGTAGCAGTGTTCTCCGCAACTGCGCACAACGATG.

**AAV-mediated gene delivery**. siRNA sequences against mouse *Fgf21* (GGGATTCAACACAGGAGAAAC) encoding siRNA, *Crebh* (TCGAGAAAAAAGACATAGCGGCTGGAAAGATCTCTTGAATCTTTCCAGCCGCTATGTCA) encoding the hairpin shRNA, and control luciferase (GTTGCGCGGAGGAGTTGTG) were cloned into pAAV8-D(+)-U6-siRNA-CMV-GFP vector via BamHI and EcoRI restriction sites. AAV was generated from these plasmids at the Harvard Children's Hospital Virus Core (Boston, MA) on a fee-for-service basis. AAV8 was injected once into 5-8-wk old mice via the tail vein at the dose of 5-10 x $10^{11}$ viral genome copies/mouse. Blood was collected via a small nick in the tail for subsequent ELISA analysis of circulating Fgf21 levels after 2 or more weeks' post injection.

**Microarray analysis**. Liver tissues were snap-frozen in liquid nitrogen. RNA was extracted as described above followed by DNaseI (New England Biolabs) digestion. RNA quality and concentration were measured using an Agilent 2100 bioanalyser. Microarray analysis was carried out as previously described (Sun, Xia et al., 2012) and will be deposited into a public database upon acceptance of the manuscript.

**Statistical Analysis**. All results have been expressed as mean ± SEM unless otherwise stated. Comparisons between groups are done by paired two-tailed Student's t test or 2-way ANOVA as needed. All experiments have been repeated at least twice or thrice, and performed with multiple independent biological samples from which representative data have been shown.



**ACKNOWLEDGEMENTS**

We thank Drs. Richard Wojcikiewicz and Yihong Ye for reagents, and Drs. Gerald Duhammel, Jiandie Lin, Peter Arvan, Robert Weiss, Kenneth Simpson, and Natasza Kurpios for insightful discussions and comments; the Histology and Vision Research Core Facilities at University of Michigan Medical School for their assistance and other members of Qi/Arvan laboratories for comments and technical assistance. This work is supported by NIH R01DK099593 (L.Y.), R01DK090313 (K.Z), R01GM113188, R01DK105393, University of Michigan Protein Folding Diseases Initiative, and American Diabetes Association (ADA) 1-12-CD-04 (L.Q.). A.B. is supported by AHA Predoctoral Fellowship grant #16PRE29750001 (2016-2018). S.S. was an International Predoctoral Fellow of the Howard Hughes Medical Institute (2012-2015) and is a Helen Hay Whitney Postdoctoral Fellow (2017-2020). L.Q. is the recipient of the Junior Faculty and Career Development Awards from American Diabetes Association (ADA).

The authors declare that they have no conflict of interest.

**AUTHOR CONTRIBUTION**

A.B. designed and performed most experiments; S.S. designed and performed experiments with human hepatocytes; H.W. and M.L. provided technical assistant; Q.L. provided reagents; S.K. performed microarray analyses; L.Y. and K.Z. provided reagents and discussion; A.B. and L.Q. wrote the manuscript; everybody commented on and approved the manuscript.

**REFERENCES**

Badman MK, Pissios P, Kennedy AR, Koukos G, Flier JS, Maratos-Flier E (2007) Hepatic fibroblast growth factor 21 is regulated by PPARalpha and is a key mediator of hepatic lipid metabolism in ketotic states. Cell Metab 5: 426-37

Bailey D, Barreca C, O'Hare P (2007) Trafficking of the bZIP transmembrane transcription factor CREB-H into alternate pathways of ERAD and stress-regulated intramembrane proteolysis. Traffic 8: 1796-814

BonDurant LD, Ameka M, Naber MC, Markan KR, Idiga SO, Acevedo MR, Walsh SA, Ornitz DM, Potthoff MJ (2017) FGF21 Regulates Metabolism Through Adipose-Dependent and -Independent Mechanisms. Cell Metab 25: 935-944 e4

Bookout AL, de Groot MH, Owen BM, Lee S, Gautron L, Lawrence HL, Ding X, Elmquist JK, Takahashi JS, Mangelsdorf DJ, Kliewer SA (2013) FGF21 regulates metabolism and circadian behavior by acting on the nervous system. Nat Med 19: 1147-52

Chan CP, Mak TY, Chin KT, Ng IO, Jin DY (2010) N-linked glycosylation is required for optimal proteolytic activation of membrane-bound transcription factor CREB-H. J Cell Sci 123: 1438-48

Chau MD, Gao J, Yang Q, Wu Z, Gromada J (2010) Fibroblast growth factor 21 regulates energy metabolism by activating the AMPK-SIRT1-PGC-1alpha pathway. Proc Natl Acad Sci U S A 107: 12553-8

De Sousa-Coelho AL, Marrero PF, Haro D (2012) Activating transcription factor 4-dependent induction of FGF21 during amino acid deprivation. Biochem J 443: 165-71

De Sousa-Coelho AL, Relat J, Hondares E, Perez-Marti A, Ribas F, Villarroya F, Marrero PF, Haro D (2013) FGF21 mediates the lipid metabolism response to amino acid starvation. J Lipid Res 54: 1786-97

Fisher FM, Kleiner S, Douris N, Fox EC, Mepani RJ, Verdeguer F, Wu J, Kharitonenkov A, Flier JS, Maratos-Flier E, Spiegelman BM (2012) FGF21 regulates PGC-1alpha and browning of white adipose tissues in adaptive thermogenesis. Genes Dev 26: 271-81

Fisher FM, Maratos-Flier E (2016) Understanding the Physiology of FGF21. Annu Rev Physiol 78: 223-41

Francisco AB, Singh R, Li S, Vani AK, Yang L, Munroe RJ, Diaferia G, Cardano M, Biunno I, Qi L, Schimenti JC, Long Q (2010) Deficiency of suppressor enhancer lin12 1 like (SEL1L) in mice leads to systemic endoplasmic reticulum stress and embryonic lethality. J Biol Chem 285: 13694-703

Fujita H, Yagishita N, Aratani S, Saito-Fujita T, Morota S, Yamano Y, Hansson MJ, Inazu M, Kokuba H, Sudo K, Sato E, Kawahara KI, Nakajima F, Hasegawa D, Higuchi I, Sato T, Araya N, Usui C, Nishioka K, Nakatani Y et al. (2015) The E3 ligase synoviolin controls body weight and mitochondrial biogenesis through negative regulation of PGC-1beta. EMBO J 34: 1042-55

Guerriero CJ, Brodsky JL (2012) The delicate balance between secreted protein folding and endoplasmic reticulum-associated degradation in human physiology. Physiol Rev 92: 537-76

Hondares E, Rosell M, Gonzalez FJ, Giralt M, Iglesias R, Villarroya F (2010) Hepatic FGF21 expression is induced at birth via PPARalpha in response to milk intake and contributes to thermogenic activation of neonatal brown fat. Cell Metab 11: 206-12

Hur KY, So JS, Ruda V, Frank-Kamenetsky M, Fitzgerald K, Koteliansky V, Iwawaki T, Glimcher LH, Lee AH (2012) IRE1alpha activation protects mice against acetaminophen-induced hepatotoxicity. J Exp Med 209: 307-18

Inagaki T, Dutchak P, Zhao G, Ding X, Gautron L, Parameswara V, Li Y, Goetz R, Mohammadi M, Esser V, Elmquist JK, Gerard RD, Burgess SC, Hammer RE, Mangelsdorf DJ, Kliewer SA (2007) Endocrine regulation of the fasting response by PPARalpha-mediated induction of fibroblast growth factor 21. Cell Metab 5: 415-25

Inagaki T, Lin VY, Goetz R, Mohammadi M, Mangelsdorf DJ, Kliewer SA (2008) Inhibition of growth hormone signaling by the fasting-induced hormone FGF21. Cell Metab 8: 77-83

Ji Y, Kim H, Yang L, Sha H, Roman CA, Long Q, Qi L (2016) The Sel1L-Hrd1 Endoplasmic Reticulum-Associated Degradation Complex Manages a Key Checkpoint in B Cell Development. Cell reports 16: 2630-40

Jiang S, Yan C, Fang QC, Shao ML, Zhang YL, Liu Y, Deng YP, Shan B, Liu JQ, Li HT, Yang L, Zhou J, Dai Z, Liu Y, Jia WP (2014) Fibroblast growth factor 21 is regulated by the IRE1alpha-XBP1 branch of the unfolded protein response and counteracts endoplasmic reticulum stress-induced hepatic steatosis. J Biol Chem 289: 29751-65

Jurczak MJ, Lee AH, Jornayvaz FR, Lee HY, Birkenfeld AL, Guigni BA, Kahn M, Samuel VT, Glimcher LH, Shulman GI (2012) Dissociation of inositol-requiring enzyme (IRE1alpha)-mediated c-Jun N-terminal kinase activation from hepatic insulin resistance in conditional X-box-binding protein-1 (XBP1) knock-out mice. J Biol Chem 287: 2558-67

Kharitonenkov A, Adams AC (2014) Inventing new medicines: The FGF21 story. Molecular metabolism 3: 221-9

Kharitonenkov A, Shiyanova TL, Koester A, Ford AM, Micanovic R, Galbreath EJ, Sandusky GE, Hammond LJ, Moyers JS, Owens RA, Gromada J, Brozinick JT, Hawkins ED, Wroblewski VJ, Li DS, Mehrbod F, Jaskunas SR, Shanafelt AB (2005) FGF-21 as a novel metabolic regulator. J Clin Invest 115: 1627-35

Kim GH, Shi G, Somlo DRM, Haataja L, Soon S, Long Q, Nillni EA, Low MJ, Arvan P, Myers MG, Qi L (2018) Hypothalamic ER-associated degradation regulates POMC maturation, feeding and age-associated obesity. J Clin Invest 128: 1125-1140

Kim H, Mendez R, Zheng Z, Chang L, Cai J, Zhang R, Zhang K (2014) Liver-enriched transcription factor CREBH interacts with peroxisome proliferator-activated receptor alpha to regulate metabolic hormone FGF21. Endocrinology 155: 769-82

Kim KH, Jeong YT, Oh H, Kim SH, Cho JM, Kim YN, Kim SS, Kim DH, Hur KY, Kim HK, Ko T, Han J, Kim HL, Kim J, Back SH, Komatsu M, Chen H, Chan DC, Konishi M, Itoh N et al. (2013a) Autophagy deficiency leads to protection from obesity and insulin resistance by inducing Fgf21 as a mitokine. Nat Med 19: 83-92

Kim KH, Kim SH, Min YK, Yang HM, Lee JB, Lee MS (2013b) Acute exercise induces FGF21 expression in mice and in healthy humans. PLoS One 8: e63517

Kong S, Yang Y, Xu Y, Wang Y, Zhang Y, Melo-Cardenas J, Xu X, Gao B, Thorp EB, Zhang DD, Zhang B, Song J, Zhang K, Zhang J, Zhang J, Li H, Fang D (2016) Endoplasmic reticulum-resident E3 ubiquitin ligase Hrd1 controls B-cell immunity through degradation of the death receptor CD95/Fas. Proc Natl Acad Sci U S A 113: 10394-9

Laeger T, Henagan TM, Albarado DC, Redman LM, Bray GA, Noland RC, Munzberg H, Hutson SM, Gettys TW, Schwartz MW, Morrison CD (2014) FGF21 is an endocrine signal of protein restriction. J Clin Invest 124: 3913-22

Lajtha A, Latzkovits L, Toth J (1976) Comparison of turnover rates of proteins of the brain, liver and kidney in mouse in vivo following long term labeling. Biochim Biophys Acta 425: 511-20

Lee AH, Scapa EF, Cohen DE, Glimcher LH (2008) Regulation of hepatic lipogenesis by the transcription factor XBP1. Science 320: 1492-6

Mehnert M, Sommermeyer F, Berger M, Kumar Lakshmipathy S, Gauss R, Aebi M, Jarosch E, Sommer T (2015) The interplay of Hrd3 and the molecular chaperone system ensures efficient degradation of malfolded secretory proteins. Mol Biol Cell 26: 185-94

Mueller B, Klemm EJ, Spooner E, Claessen JH, Ploegh HL (2008) SEL1L nucleates a protein complex required for dislocation of misfolded glycoproteins. Proc Natl Acad Sci USA 105: 12325-30

Murgatroyd C, Hoffmann A, Spengler D (2012) In vivo ChIP for the analysis of microdissected tissue samples. Methods Mol Biol 809: 135-48

Nakagawa Y, Satoh A, Yabe S, Furusawa M, Tokushige N, Tezuka H, Mikami M, Iwata W, Shingyouchi A, Matsuzaka T, Kiwata S, Fujimoto Y, Shimizu H, Danno H, Yamamoto T, Ishii K, Karasawa T, Takeuchi Y, Iwasaki H, Shimada M et al. (2014) Hepatic CREB3L3 controls whole-body energy homeostasis and improves obesity and diabetes. Endocrinology 155: 4706-19

Olivares S, Henkel AS (2015) Hepatic Xbp1 Gene Deletion Promotes Endoplasmic Reticulum Stress-induced Liver Injury and Apoptosis. J Biol Chem 290: 30142-51

Omori Y, Imai J, Watanabe M, Komatsu T, Suzuki Y, Kataoka K, Watanabe S, Tanigami A, Sugano S (2001) CREB-H: a novel mammalian transcription factor belonging to the CREB/ATF family and functioning via the box-B element with a liver-specific expression. Nucleic Acids Res 29: 2154-62

Owen BM, Ding X, Morgan DA, Coate KC, Bookout AL, Rahmouni K, Kliewer SA, Mangelsdorf DJ (2014) FGF21 acts centrally to induce sympathetic nerve activity, energy expenditure, and weight loss. Cell Metab 20: 670-7

Park JG, Xu X, Cho S, Hur KY, Lee MS, Kersten S, Lee AH (2016a) CREBH-FGF21 axis improves hepatic steatosis by suppressing adipose tissue lipolysis. Sci Rep 6: 27938

Park JG, Xu X, Cho S, Lee AH (2016b) Loss of Transcription Factor CREBH Accelerates Diet-Induced Atherosclerosis in Ldlr-/- Mice. Arterioscler Thromb Vasc Biol 36: 1772-81

Potthoff MJ, Kliewer SA, Mangelsdorf DJ (2012) Endocrine fibroblast growth factors 15/19 and 21: from feast to famine. Genes Dev 26: 312-24

Qi L, Tsai B, Arvan P (2017) New Insights into the Physiological Role of Endoplasmic Reticulum-Associated Degradation. Trends Cell Biol 27: 430-440

Qi L, Yang L, Chen H (2011) Detecting and quantitating physiological endoplasmic reticulum stress. Meth Enzymol 490: 137-146

Schaap FG, Kremer AE, Lamers WH, Jansen PL, Gaemers IC (2013) Fibroblast growth factor 21 is induced by endoplasmic reticulum stress. Biochimie 95: 692-9

Sha H, He Y, Chen H, Wang C, Zenno A, Shi H, Yang X, Zhang X, Qi L (2009) The IRE1alpha-XBP1 pathway of the unfolded protein response is required for adipogenesis. Cell Metab 9: 556-64

Sha H, Sun S, Francisco AB, Ehrhardt N, Xue Z, Liu L, Lawrence P, Mattijssen F, Guber RD, Panhwar MS, Brenna JT, Shi H, Xue B, Kersten S, Bensadoun A, Peterfy M, Long Q, Qi L (2014) The ER-associated degradation adaptor protein Sel1L regulates LPL secretion and lipid metabolism. Cell Metab 20: 458-70

Shi G, Somlo D, Kim GH, Prescianotto-Baschong C, Sun S, Beuret N, Long Q, Rutishauser J, Arvan P, Spiess M, Qi L (2017) ER-associated degradation is required for vasopressin prohormone processing and systemic water homeostasis. J Clin Invest 127: 3897-3912

So JS, Hur KY, Tarrio M, Ruda V, Frank-Kamenetsky M, Fitzgerald K, Koteliansky V, Lichtman AH, Iwawaki T, Glimcher LH, Lee AH (2012) Silencing of Lipid Metabolism Genes through IRE1alpha-Mediated mRNA Decay Lowers Plasma Lipids in Mice. Cell Metab 16: 487-99

Sun S, Louri R, Cohen SB, Ji Y, Goodrich JK, Poole AC, Ley RE, Denkers EY, Mcguckin MA, Long Q, Duhamel GE, Simpson KW, Qi L (2016) Epithelial Sel1L is required for the maintenance of intestinal homeostasis. Mol Biol Cell 27: 483-90

Sun S, Shi G, Han X, Francisco AB, Ji Y, Mendonca N, Liu X, Locasale JW, Simpson KW, Duhamel GE, Kersten S, Yates JR, 3rd, Long Q, Qi L (2014) Sel1L is indispensable for mammalian endoplasmic reticulum-associated degradation, endoplasmic reticulum homeostasis, and survival. Proc Natl Acad Sci U S A 111: E582-591

Sun S, Shi G, Sha H, Ji Y, Han X, Shu X, Ma H, Inoue T, Gao B, Kim H, Bu P, Guber RD, Shen X, Lee AH, Iwawaki T, Paton AW, Paton JC, Fang D, Tsai B, Yates Iii JR et al. (2015) IRE1a is an endogenous substrate of endoplasmic-reticulum-associated degradation. Nat Cell Biol 17: 1546-1555

Sun S, Xia S, Ji Y, Kersten S, Qi L (2012) The ATP-P2X7 Signaling Axis Is Dispensable for Obesity-Associated Inflammasome Activation in Adipose Tissue. Diabetes 61: 1471-8

Vashistha N, Neal SE, Singh A, Carroll SM, Hampton RY (2016) Direct and essential function for Hrd3 in ER-associated degradation. Proc Natl Acad Sci U S A 113: 5934-9

Vecchi C, Montosi G, Zhang K, Lamberti I, Duncan SA, Kaufman RJ, Pietrangelo A (2009) ER stress controls iron metabolism through induction of hepcidin. Science 325: 877-80

Wan XS, Lu XH, Xiao YC, Lin Y, Zhu H, Ding T, Yang Y, Huang Y, Zhang Y, Liu YL, Xu ZM, Xiao J, Li XK (2014) ATF4- and CHOP-dependent induction of FGF21 through endoplasmic reticulum stress. Biomed Res Int 2014: 807874

Wu T, Zhao F, Gao B, Tan C, Yagishita N, Nakajima T, Wong PK, Chapman E, Fang D, Zhang DD (2014) Hrd1 suppresses Nrf2-mediated cellular protection during liver cirrhosis. Genes Dev 28: 708-22

Xu X, Park JG, So JS, Hur KY, Lee AH (2014) Transcriptional regulation of apolipoprotein A-IV by the transcription factor CREBH. J Lipid Res 55: 850-9
Xu Y, Zhao F, Qiu Q, Chen K, Wei J, Kong Q, Gao B, Melo-Cardenas J, Zhang B, Zhang J, Song J, Zhang DD, Zhang J, Fan Y, Li H, Fang D (2016) The ER membrane-anchored ubiquitin ligase Hrd1 is a positive regulator of T-cell immunity. Nature communications 7: 12073
Yagishita N, Ohneda K, Amano T, Yamasaki S, Sugiura A, Tsuchimochi K, Shin H, Kawahara K, Ohneda O, Ohta T, Tanaka S, Yamamoto M, Maruyama I, Nishioka K, Fukamizu A, Nakajima T (2005) Essential role of synoviolin in embryogenesis. J Biol Chem 280: 7909-16
Yang H, Qiu Q, Gao B, Kong S, Lin Z, Fang D (2014) Hrd1-mediated BLIMP-1 ubiquitination promotes dendritic cell MHCII expression for CD4 T cell priming during inflammation. J Exp Med 211: 2467-79
Yang L, Xue Z, He Y, Sun S, Chen H, Qi L (2010) A Phos-tag-based method reveals the extent of physiological endoplasmic reticulum stress. PLos ONE 5: e11621
Zhang C, Wang G, Zheng Z, Maddipati KR, Zhang X, Dyson G, Williams P, Duncan SA, Kaufman RJ, Zhang K (2012) Endoplasmic reticulum-tethered transcription factor cAMP responsive element-binding protein, hepatocyte specific, regulates hepatic lipogenesis, fatty acid oxidation, and lipolysis upon metabolic stress in mice. Hepatology 55: 1070-82
Zhang K, Shen X, Wu J, Sakaki K, Saunders T, Rutkowski DT, Back SH, Kaufman RJ (2006) Endoplasmic reticulum stress activates cleavage of CREBH to induce a systemic inflammatory response. Cell 124: 587-99
Zhang K, Wang S, Malhotra J, Hassler JR, Back SH, Wang G, Chang L, Xu W, Miao H, Leonardi R, Chen YE, Jackowski S, Kaufman RJ (2011) The unfolded protein response transducer IRE1alpha prevents ER stress-induced hepatic steatosis. Embo J 30: 1357-75
Zhang Y, Xie Y, Berglund ED, Coate KC, He TT, Katafuchi T, Xiao G, Potthoff MJ, Wei W, Wan Y, Yu RT, Evans RM, Kliewer SA, Mangelsdorf DJ (2012) The starvation hormone, fibroblast growth factor-21, extends lifespan in mice. eLife 1: e00065
Zhao Y, Dunbar JD, Kharitonenkov A (2012) FGF21 as a therapeutic reagent. Adv Exp Med Biol 728: 214-28
Zhu S, Ma L, Wu Y, Ye X, Zhang T, Zhang Q, Rasoul LM, Liu Y, Guo M, Zhou B, Ren G, Li D (2014) FGF21 treatment ameliorates alcoholic fatty liver through activation of AMPK-SIRT1 pathway. Acta biochimica et biophysica Sinica 46: 1041-8

**MAIN FIGURES AND LEGENDS**

**Figure 1. Liver-specific Sel1L deficiency in mice (*Sel1L*$^{Alb}$) causes growth retardation.**

(A) Western blot analysis and quantitation of Sel1L-Hrd1 ERAD proteins in the livers of WT mice at 3, 9 and 24 weeks of age (n=3-6 per group, 2 independent repeats).

(B) Western blot analysis and quantitation of Sel1L-Hrd1 ERAD proteins in the livers of 10-week-old WT mice under fasted (overnight) or ad libitum fed conditions (n=3-6 per group, 2 independent repeats).

(C) Western blot analysis and quantitation of ERAD proteins in *Sel1L*$^{f/f}$ and *Sel1L*$^{Alb}$ livers (n=4 per group, 3 independent repeats).

(D) Growth curves of male (n=10 each) and female (n=7 each) mice.

(E-F) Representative images (E) and nose-to-anus length (F) of male mice at 6 weeks of age (n=6-10 per group).

(G) Organ-to-body-weight ratios of liver and kidney in 6-week-old male mice (n=6 per group, 3 independent repeats).

(H) Daily food intake (g/d) normalized to gram of body weight (gbw) (n=3 per group, measured over 3 days).

(I) Representative estrus cycle mapping in 2-4-month old females (n=6 per group).

(J) H&E images of paraffin-embedded liver sections from 9-week-old mice (n=4 per group, 3 independent repeats).

(K) Western blot analysis of cell death (cleaved and pro-caspase-3) in livers of 9-week-old mice, with WT ileum as positive control (n=3 per group, 3 independent repeats).

(L) Representative transmission electron microscope (TEM) images obtained from 9-week-old female mice livers (n=10-12 cells from one mouse each). N, nucleus; mito, mitochondria; ER, endoplasmic reticulum.

Data information: Hsp90 and α-tubulin, loading controls for Western blot analysis. Values are mean ± SEM; *, p<0.05; **, p<0.01; ***, p<0.001, n.s., non-significant by Student's t test.

**Figure 2. Elevated *Fgf21* expression in the liver as well as circulating Fgf21 in the absence of Sel1L.**

(A) Volcano plot depicting transcriptomics data from the livers of 9-week-old *Sel1L*$^{f/f}$ and *Sel1L*$^{Alb}$ mice (n=3 per group); dotted line marks p=0.05; black dots represent fold change>2.

(B-C) qPCR (B) and Western blot (C) analyses of *Fgf21* expression in 9-week-old livers (n=3-6 per group, 3 independent repeats).

(D) ELISA analysis of Fgf21 in serum from 8-9-week-old mice (n=6-7 per group).

(E) Protein levels of Sel1L (left panel) and mRNA levels of Fgf21 (right panel) in primary mouse hepatocytes isolated from the tamoxifen-inducible Sel1L-knockout *Sel1L*$^{ERCre}$ mice (2 independent repeats).
(F-G) Acute loss-of-function model where 8-week-old *Sel1L*$^{f/f}$ mice were injected i.v. with either AAV8-Cre or control AAV8-GFP: (F) Western blot analysis of hepatic and control adipose Sel1L protein (n=3 per group); and (G) qPCR analysis of hepatic *Fgf21* expression and ELISA analysis of serum Fgf21 (n=3 per group, 2 independent repeats).
(H) Heatmaps of top 15 significantly upregulated and downregulated genes in *Fgf21 Tg* livers and their expression levels in *Sel1L*$^{Alb}$ livers (n=3 per group).
(I) Scatter plot depicting the logarithmic fold-change (FC) for 16,402 genes in *Sel1L*$^{Alb}$ and *Fgf21* transgenic *(Tg)* livers (n=3 per group); genes that are highly upregulated or downregulated in both datasets are marked in red and blue, respectively; genes that are upregulated unique to each data set (e.g. *Derl3* for Sel1L-Hrd1 ERAD-deficient liver) are marked in green.
(J-L) Data from rescue experiments where 5-week-old *Sel1L*$^{f/f}$ and *Sel1L*$^{Alb}$ mice were injected i.v. with AAV8-*shFgf21* or control AAV8-*shLuc*: (J-K) qPCR analysis of *Fgf21* mRNA (J) and ELISA analysis of Fgf21 in serum (K) 3 weeks after injection (n=4 per group). (L) Weight gain curve after injection (n=7 per group).
Data information: Hsp90 and α-tubulin, loading control for Western blot analysis. Ribosomal *L32*, loading control for qPCR analysis. Values are mean ± SEM; *, p<0.05; **, p<0.01; ***, p<0.001, n.s., non-significant by Student's t test (B-G) or 2-way ANOVA analysis (J-L).

**Figure 3. *Sel1L*$^{Alb}$ mice phenocopy Fgf21-gain-of-function mice.**
(A) Western blot analysis of p-Stat5 in livers of 9-week-old mice (n=3 per group, 3 independent repeats), with quantitation of the ratio of p- to total Stat5 shown below the blot.
(B) qPCR analysis of p-Stat5-associated growth genes in the livers of 9-week-old mice (n=6 per group, 2 independent repeats).
(C) Z ambulatory activity of 9-week-old male mice as measured over 24 hr (n=4 males per group).
(D-G) Blood glucose (D), serum insulin (E), serum triglyceride (TG) (F), serum cholesterol (CHOL) (G) levels in 9-week-old mice after 6 hr fasting (n=6-10 per group).
(H) H&E images of inguinal white adipose tissue (iWAT) from 8-week-old mice (n=3 per group, 2 independent repeats).
(I) qPCR analysis of browning-related genes in iWAT (n=3-6 per group).

(J) Western blot analysis of Ucp1 in iWAT of 8-week-old mice (n=3-4 per group, 3 independent repeats).
(K) Weight gain curve of male mice after 60% high fat diet (HFD) starting at 5 weeks of age (n=4 per group, 2 independent repeats).
(L) Adipose tissue weight normalized to body weight in male mice following 9 weeks of HFD feeding (n=4 per group).
Data information: Hsp90, loading control for Western blot analysis. Ribosomal *L32*, loading control for qPCR analysis. Values are mean ± SEM; *, p<0.05; **, p<0.01; ***, p<0.001 by Student's t test or 2-way ANOVA, as needed.

**Figure 4. Sel1L deficiency leads to the accumulation of Crebh in the liver.**
(A-C) Western blot analysis of Crebh, Crebh-N, Pparα and Xbp1s in whole cell lysates (A) and nuclear extracts (B) in WT and *Sel1L*$^{Alb}$ livers (n=3 per group, 3 independent repeats) with quantitation shown in (C).
(D) qPCR analysis of *Crebh*, *Ppara* and *Xbp1s* in WT and *Sel1L*$^{Alb}$ livers (n=4-6 per group, 2 independent repeats).
(E) Western blot analysis of Crebh in acute Sel1L loss of function model as described in Figure 2F-G (n=3 per group).
(F) Western blot analysis of Crebh protein in 9-week-old mice (n=3 per group, 2 independent repeats). WT mice injected i.p. with tunicamycin (Tm, 1.5 µg/g body weight) for 72 hours were included as a control.
(G) Western blot analysis of Crebh in the livers of 9-week-old mice after NP40-detergent fractionation into NP40 soluble (NP40S) and pellet (NP40P) (n=3 per group, 2 independent repeats).
(H) Representative confocal images of Crebh in the liver cryosections of 8-week-old mice (zoomed out versions in Figure EV3F). Note that a fraction of hepatocytes is binucleated. Yellow arrows represent Crebh staining inside in the hepatocyte nucleus.
(I) ChIP analysis of Crebh binding onto the *Fgf21* promoter in the livers of 9-week-old mice, normalized first to 5% input group and then to no-antibody ChIP samples (n=3 pooled per group, 2 independent repeats).
(J-K) Western blot analysis of SEL1L, HRD1 and CREBH proteins (J) and qPCR analysis of *SEL1L*, *HRD1* and *FGF21* (K) in human Hep3B hepatocytes upon CRISPR deletion of SEL1L with two different guides.

Data information: Hsp90, H2A, β-actin and lamin, loading controls for Western blot analysis. Ribosomal *L32*, loading control for qPCR analysis. Values are mean ± SEM; *, p<0.05; **, p<0.01; ***, p<0.001; n.s., non-significant by Student's t test.

**Figure 5. Crebh is an Sel1L-Hrd1 ERAD substrate**.

(A) Western blot analysis of Crebh protein half-life in transfected WT and HRD1-/- HEK293T cells treated with cycloheximide (CHX) for indicated times. The decay of protein from one experiment is shown below.

(B-C) Western blot analysis and quantitation of Crebh in Crebh-transfected WT (B) and *HRD1-/-* (C) HEK293T cells pre-treated with the proteasomal inhibitor bortezomib (BTZ) or lysosomal inhibitor chloroquine (CHQ) for 2 hours and then with CHX for additional 1 hour (n=2 per group, 2 independent repeats).

(D) Western blot analysis of Crebh ubiquitination following immunoprecipitation (IP) of Crebh-Flag and Crebh-N-Flag in HEK293T cells transfected with indicated plasmids. Samples were boiled with SDS before IP for denaturing IP and not so for native IP. These cells were treated with proteasomal inhibitor BTZ for the last 6 hr prior to immunoprecipitation.

(E) Western blot analysis of endoglycosidase H (endoH)-sensitivity of Crebh in the livers of 9-week-old mice; 'r' refers to endoH-cleavage-resistant species and 's' refers to endoH-cleavage-sensitive species (n=3 per group, 2 independent repeats).

Data information: Hsp90, loading control for Western blot analysis. Values are mean ± SEM; *, p<0.05; **, p<0.01; n.s., non-significant by 2-way ANOVA analysis.

**Figure 6. Crebh links hepatic Sel1L-Hrd1 ERAD to Fgf21**.

5-week-old *Sel1L*$^{f/f}$ and *Sel1L*$^{Alb}$ mice were injected i.v. once with AAV8-*shCrebh* or control AAV8-*shLuc*.

(A) Western blot analysis of hepatic Sel1L and Crebh 5 weeks post injection (n=3 mice each, 2 independent repeats).

(B-C) qPCR analysis of *Crebh* and *Fgf21* mRNA (B) and ELISA analysis of circulating Fgf21 (C) 5 weeks post injection (n=3 per group, 2 independent repeats).

(D) qPCR analysis of hepatic growth-associated genes 5 weeks after injection (n=6 per group).

(E) Weight gain 6 weeks post injection (n=10 per group).

(F) Insulin tolerance test (ITT) 5-weeks after injection (n=10 per group).

(G-H) qPCR (G) and Western blot analysis (H) of Ucp1 levels in inguinal white adipose tissue (iWAT) 5 weeks post injection (n=3 per group, 2 independent repeats).

Data information: Hsp90, loading control for Western blot analysis. Ribosomal *L32*, loading control for qPCR analysis. Values are mean ± SEM; *, p<0.05; **, p<0.01; ***, p<0.001; n.s., non-significant by 2-way ANOVA analysis (B-G) and Student's t test (A,H).

**Figure 7. Sel1L-Hrd1 ERAD represses Crebh and Fgf21 under fasting-feeding and growth.**
Analysis of correlation between Sel1L-Hrd1 ERAD and Crebh-Fgf21 during fasting-feeding (A-D) and growth (E-H).
(A) Western blot analysis of hepatic Sel1L-Hrd1 ERAD and Crebh of nuclear (Nuc) and cytosolic (Cyto) fractions from 10-week-old *Sel1L*$^{f/f}$ and *Sel1L*$^{Alb}$ mice under overnight fasted or fed states.
(B) Quantitation of levels of Sel1L/Hrd1/Crebh proteins and *Fgf21* mRNA in the livers of 10-week-old *Sel1L*$^{f/f}$ mice.
(C) Quantitation of total Crebh (Crebh+Crebh-N) protein levels in the livers of 10-week-old *Sel1L*$^{f/f}$ and *Sel1L*$^{Alb}$ mice.
(D) Serum Fgf21 levels in 10-week-old *Sel1L*$^{f/f}$ and *Sel1L*$^{Alb}$ mice.
(E-H) Similar to (A-D) with the exception that these experiments were done with the livers from *Sel1L*$^{f/f}$ and *Sel1L*$^{Alb}$ mice at 3, 9 and 24 weeks of age.
Data information: Hsp90 and lamin, loading controls for cytosolic and nuclear fractions. Values are mean ± SEM; **, p<0.01 by two-way ANOVA analysis. n=3-4 per group, 2 independent repeats.

**Figure 8. Model: Hepatic Sel1L-Hrd1 ERAD regulates systemic metabolism via modulation of the "Crebh-Fgf21" axis in physiological contexts.**
Model depicting how physiological signals such as growth and fasting-feeding are integrated at the ER membrane via the Sel1L-Hrd1 ERAD complex in liver to regulate CREBH protein turnover at the ER membrane, and *Fgf21* transcription and metabolic states in the body. New findings elucidated by this study are highlighted in red arrows.

## EXPANDED VIEW FIGURES AND LEGENDS

**Figure EV1. Lack of cell death, inflammation and overt ER stress in Sel1L-deficient hepatocytes**.

(A) TUNEL staining of paraffin-embedded livers of 9-week-old mice with quantitation shown on the right (n=4 per group, 2 independent repeats).

(B) qPCR analysis of inflammation associated hepatic gene expression in *Sel1L*$^{f/f}$ and *Sel1L*$^{Alb}$ mice (n=4 per group, 3 independent repeats).

(C) Western blot analysis of Sel1L and UPR proteins (Ire1α and BiP) in the livers of 9-week-old mice (n=3 per group, 3 independent repeats). +/- Gly refers to proteins with or without glycosylation; and p/0 refers to phosphorylated or non-phosphorylated Ire1α. WT mice injected i.p. with tunicamycin (Tm, 1.5 μg/g body weight) for 72 hours were included as a control.

(D) RT-PCR analysis of *Xbp1* splicing in the livers of 9-week-old mice (n=3 per group, 3 independent repeats); u/s/t refers to unspliced/spliced/total *Xbp1*. WT mice injected i.p. with tunicamycin (Tm, 1.5 μg/g body weight) for 72 hours were included as a control.

(E) RT-PCR analysis of *Xbp1* splicing in primary mouse hepatocytes (n=2 per group, 2 independent repeats). WT primary hepatocytes treated with 200 nM thapsigargin (Tg) for 6 hours were included as a control. Quantitation of the percent of Xbp1s in total Xbp1 mRNA is shown below.

Data information: Hsp90, loading control for Western blot analysis. Ribosomal *L32*, loading control for qPCR and RT-PCR analysis. Values are mean ± SEM; *, $p<0.05$; **, $p<0.01$; n.s., not significant by Student's t test.

**Figure EV2. Hepatic Sel1L-Hrd1 ERAD deficient mice have altered metabolism.**

(A) qPCR analysis of lipid synthesis and transport genes in 9-week-old mice (n=6 per group, 2 independent repeats).

(B) Serum glucagon levels after 6 hr of fast in the morning (n=5-6 per group).

(C-D) Insulin tolerance test (ITT) (C) and glucose tolerance test (GTT) (D) of 10-week-old male mice (n=6 per group).

(E) Insulin tolerance test (ITT) 3 weeks after i.v. injection (n=5-6 per group) with AAV8-*shFgf21* or control AAV8-*shLuc*.

Data information: Ribosomal *L32*, loading control for qPCR analysis. Values are mean ± SEM; *, $p<0.05$; **, $p<0.01$; n.s., non-significant by Student's t test.

**Figure EV3. Hepatic Sel1L regulates protein stability and activity of Crebh, not Pparα.**

(A) Schematic diagram showing the intracellular trafficking of ER-resident Crebh protein to the Golgi for proteolysis, leading to the generation of Crebh-N. Crebh-N subsequently translocates into the nucleus to activate gene transcription.

(B-C) qPCR analysis of Crebh (B) and Pparα (C) target genes in WT and *Sel1L*$^{Alb}$ livers of 9-week-old mice (n=4 per group, 2 independent repeats).

(D) qPCR analysis of hepatic *Fgf21* expression in the livers of 9-week-old *Sel1L*$^{f/f}$ and *Sel1L*$^{Alb}$ mice (n=3 per group, 2 independent repeats). WT mice injected i.p. with tunicamycin (Tm, 1.5 μg/g body weight) for 72 hr were included as a control.

(E) qPCR analysis of *Fgf21* expression in primary hepatocytes (n=2 per group, 2 independent repeats). WT primary hepatocytes treated with 200 nM thapsigargin (Tg) for 6 hr are included as a control.

(F) Representative immunostaining images (zoomed out from Figure 4H) from 8-week-old liver cryosections.

Data information: Ribosomal *L32*, loading control for qPCR analysis. Values are mean ± SEM; *, $p<0.05$; **, $p<0.01$; ***, $p<0.001$ by Student's t test.

**Figure EV4. Crebh, and not Crebh-N, is an ERAD substrate.**

(A-B) Western blot analysis of Crebh (A) and cleavage-defective-Crebh (B, Crebh*) half-life in transfected *WT, Sel1L-/-* and *Hrd1-/-* N2a cells treated with cycloheximide (CHX) for indicated times. The decay of Crebh proteins is shown below.

(C) Representative immunostaining images of transfected Crebh-N-Flag protein 24-hr post transfection into *WT* and *HRD1-/-* HEK293T cells.

(D) Western blot analysis and quantitation of Crebh-N protein decay in Crebh-N-Flag-transfected *WT* and *HRD1-/-* HEK293T cells with cycloheximide (CHX) treatment for the indicated times, with quantitiation shown below.

(E-F) Co-immunoprecipitation analysis of Crebh with Hrd1 (E) and Sel1L (F) when co-expressed in HEK293T cells.

Data information: All cell culture experiments were done in 2-3 independent repeats with cells passaged less than 3 times. Hsp90, loading control for Western blot analysis.

**Figure EV5. Crebh deletion does not affect ER stress level in *Sel1L*$^{Alb}$ liver.**

(A) Representative images of livers from *Sel1L*$^{f/f}$ and *Sel1L*$^{Alb}$ mice (n=6 per group) post AAV-shRNA-GFP injection showing green (GFP positive) livers.
(B-D) Western blot analysis (B), qPCR analysis (C) and RT-PCR analysis of *Xbp1* mRNA splicing (D) of hepatic UPR markers in *Sel1L*$^{f/f}$ and *Sel1L*$^{Alb}$ mice 5 weeks post one i.v. AAV8-*shCrebh* or control AAV8-*shLuc* injection (n=3 per group, 2 independent repeats). Quantitation of protein levels (B) and the percent of Xbp1s in total Xbp1 mRNA (D) is shown below. WT mice injected i.p. with tunicamycin (Tm, 1.5 μg/g body weight) for 72 hr were included as a control.
(E) Weekly weight gain post i.v. injection (n=10 per group) with AAV8-*shFgf21* or control AAV8-*shLuc*.
Data information: Hsp90, loading control for Western blot analysis. Ribosomal *L32*, loading control for qPCR analysis. Values are mean ± SEM; *, $p<0.05$; **, $p<0.01$; ***, $p<0.001$, n.s., non-significant by 2-way ANOVA analysis.

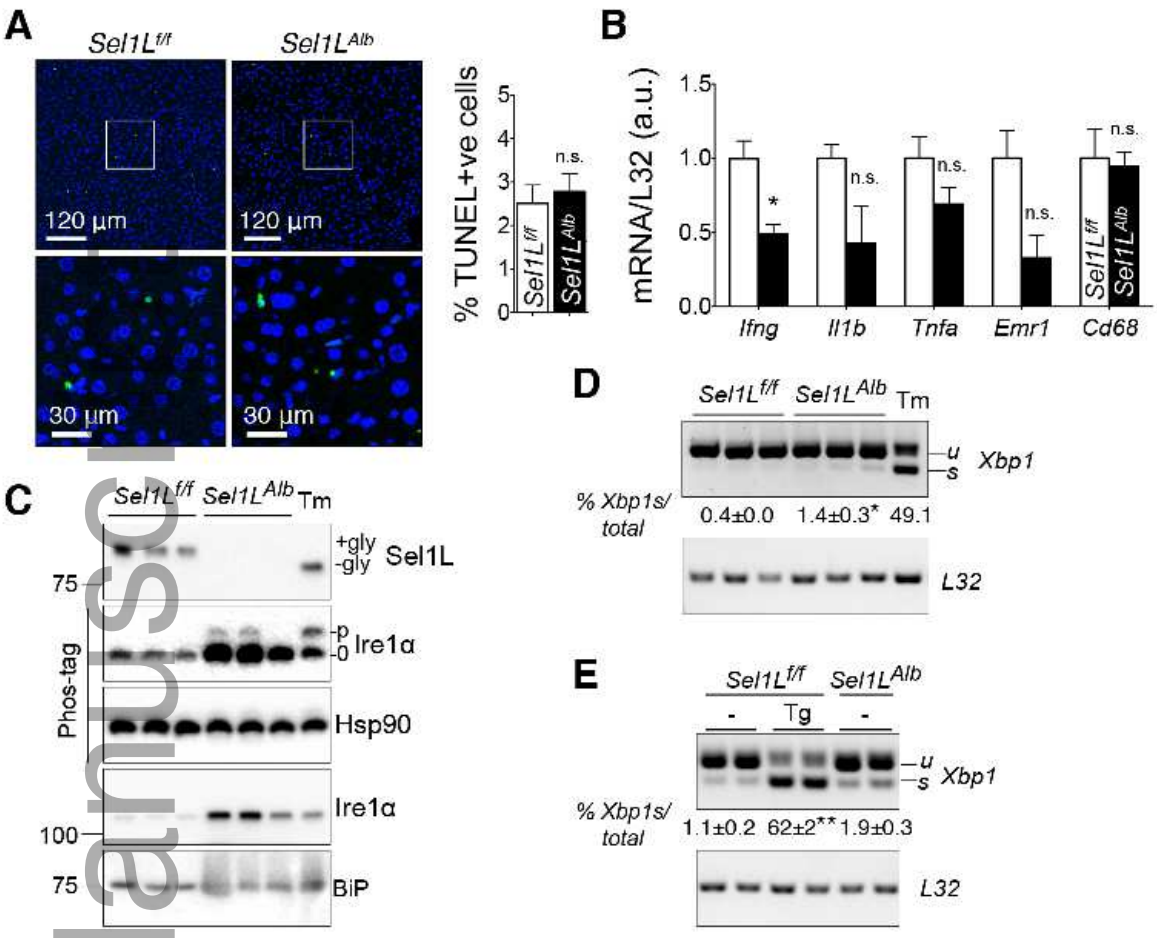


embj_201899277_f1ev.tif

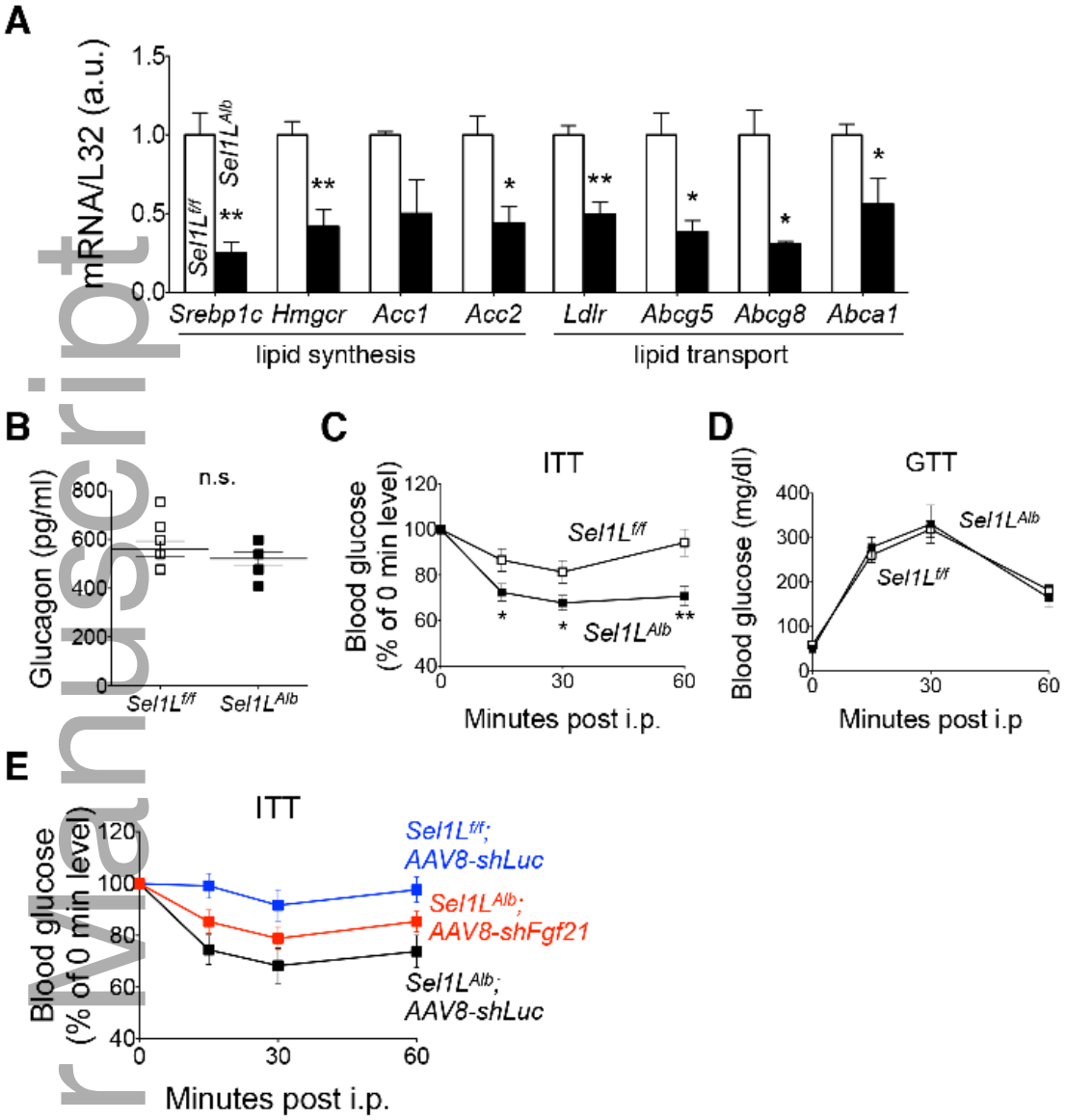


embj_201899277_f2ev.tif

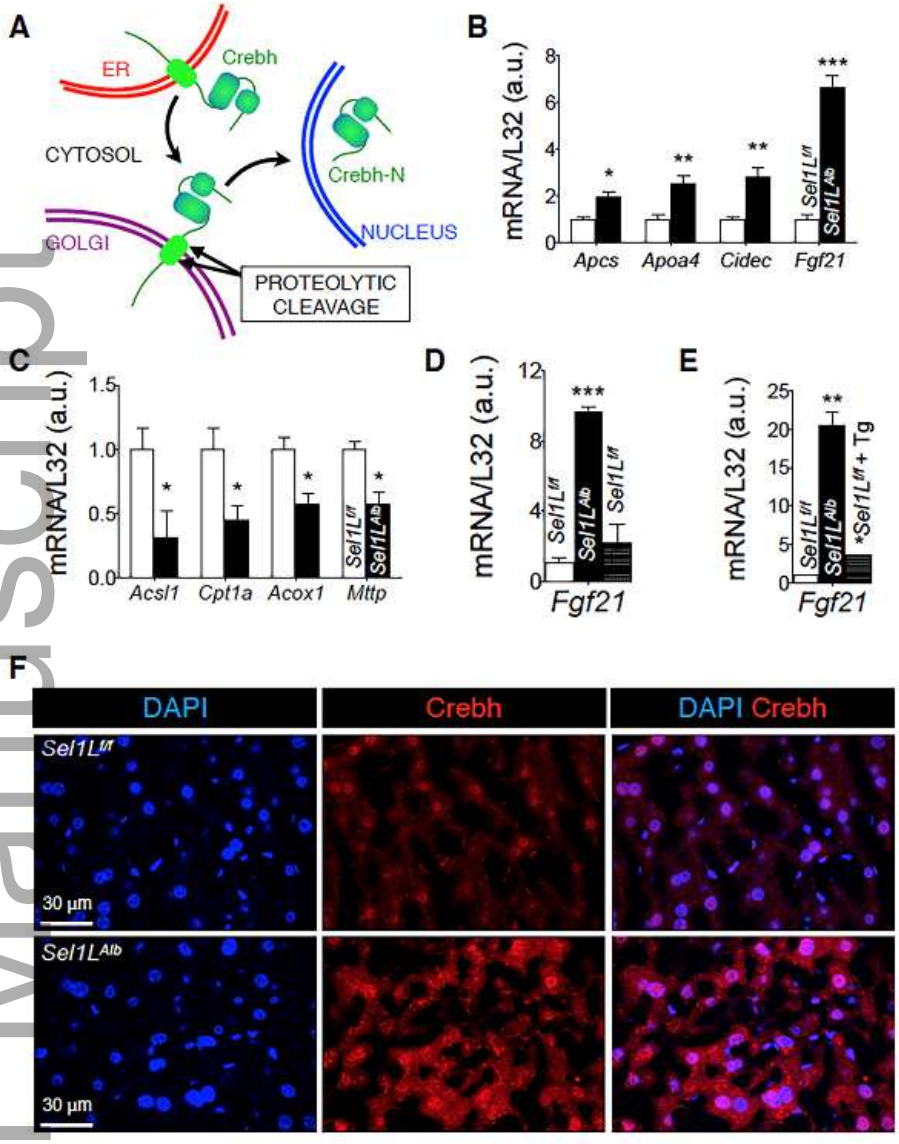


embj_201899277_f3ev.tif

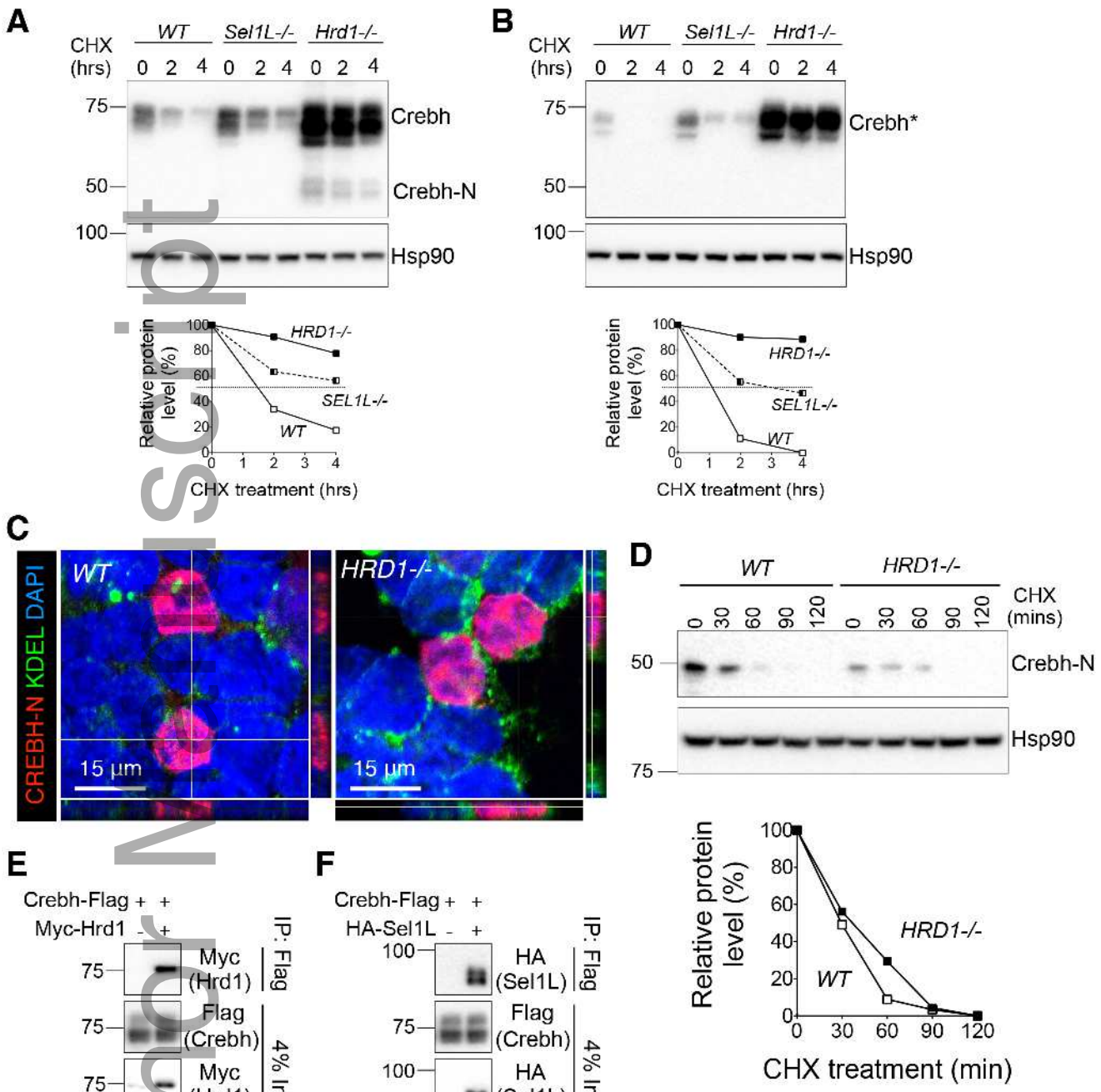


embj_201899277_f4ev.tif

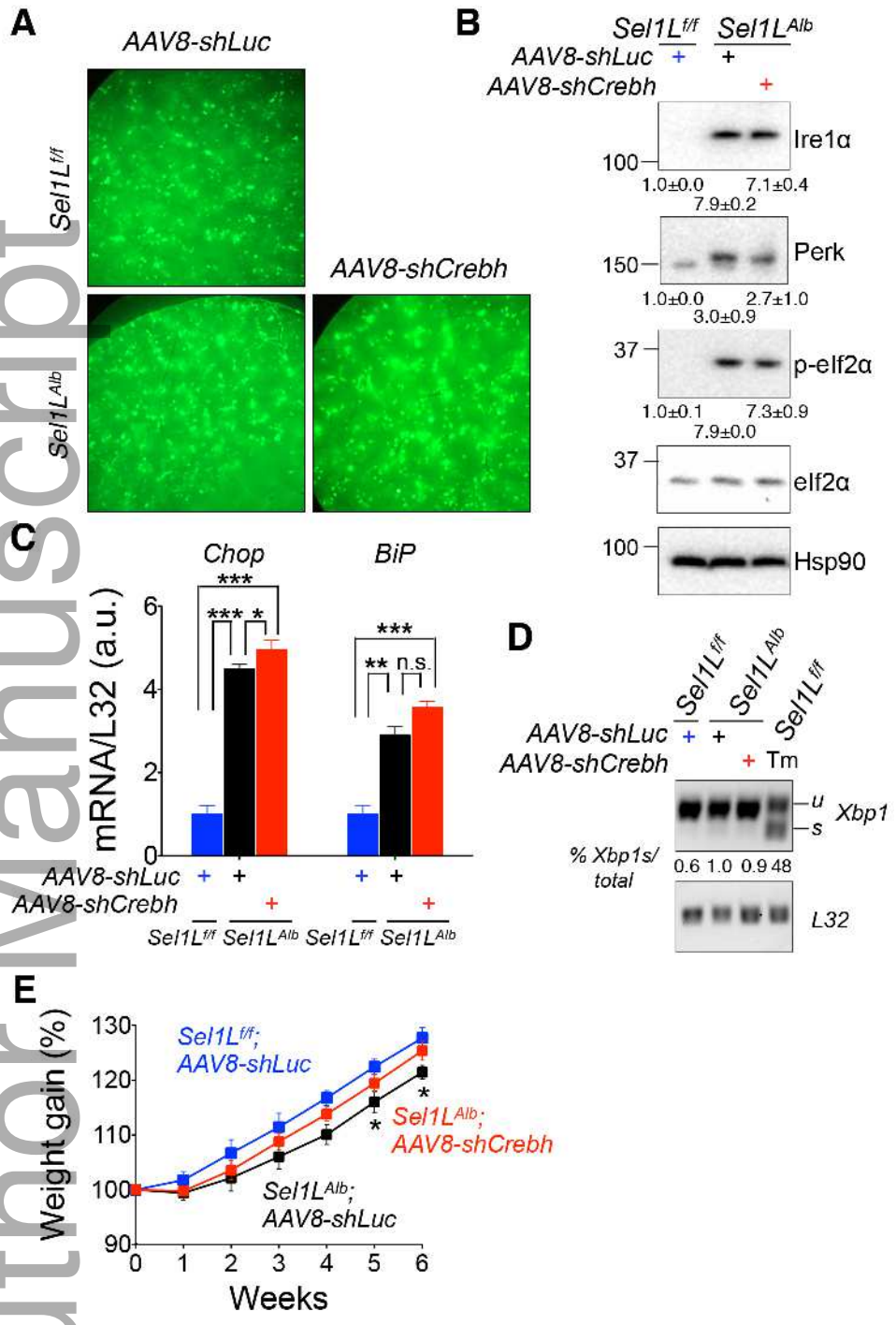


embj_201899277_f5ev.tif

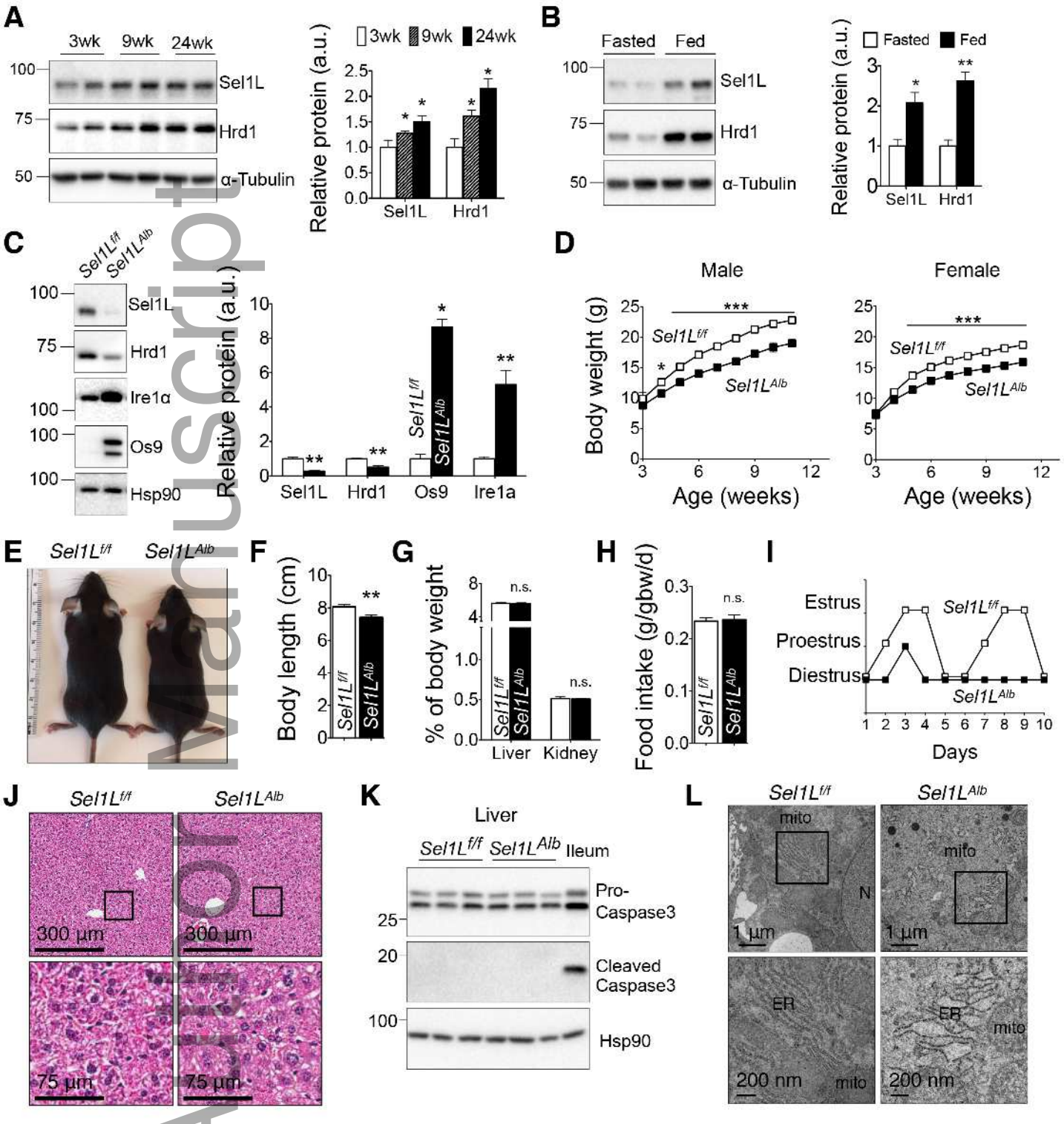




embj_201899277_f1.tif

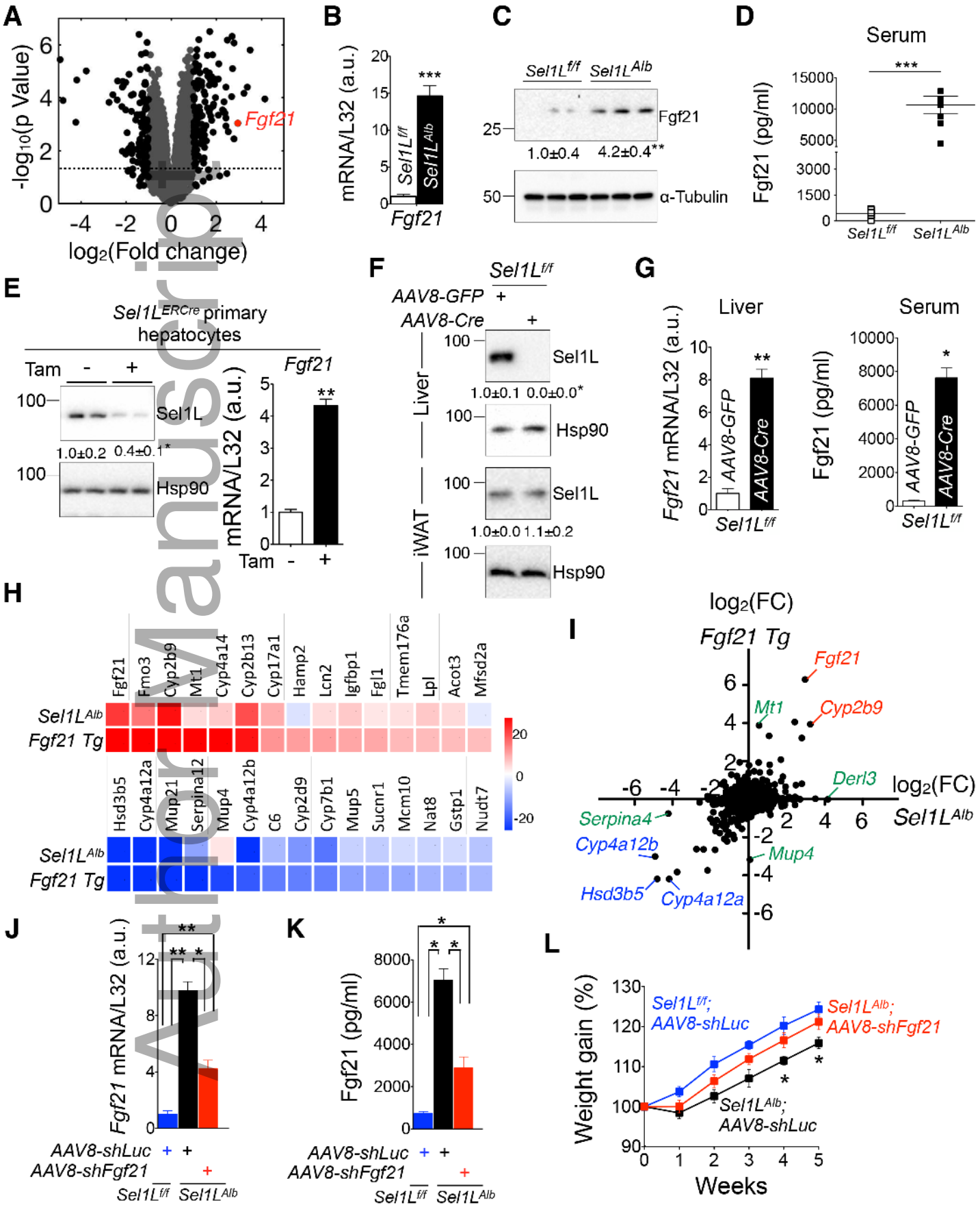




embj_201899277_f2.tif

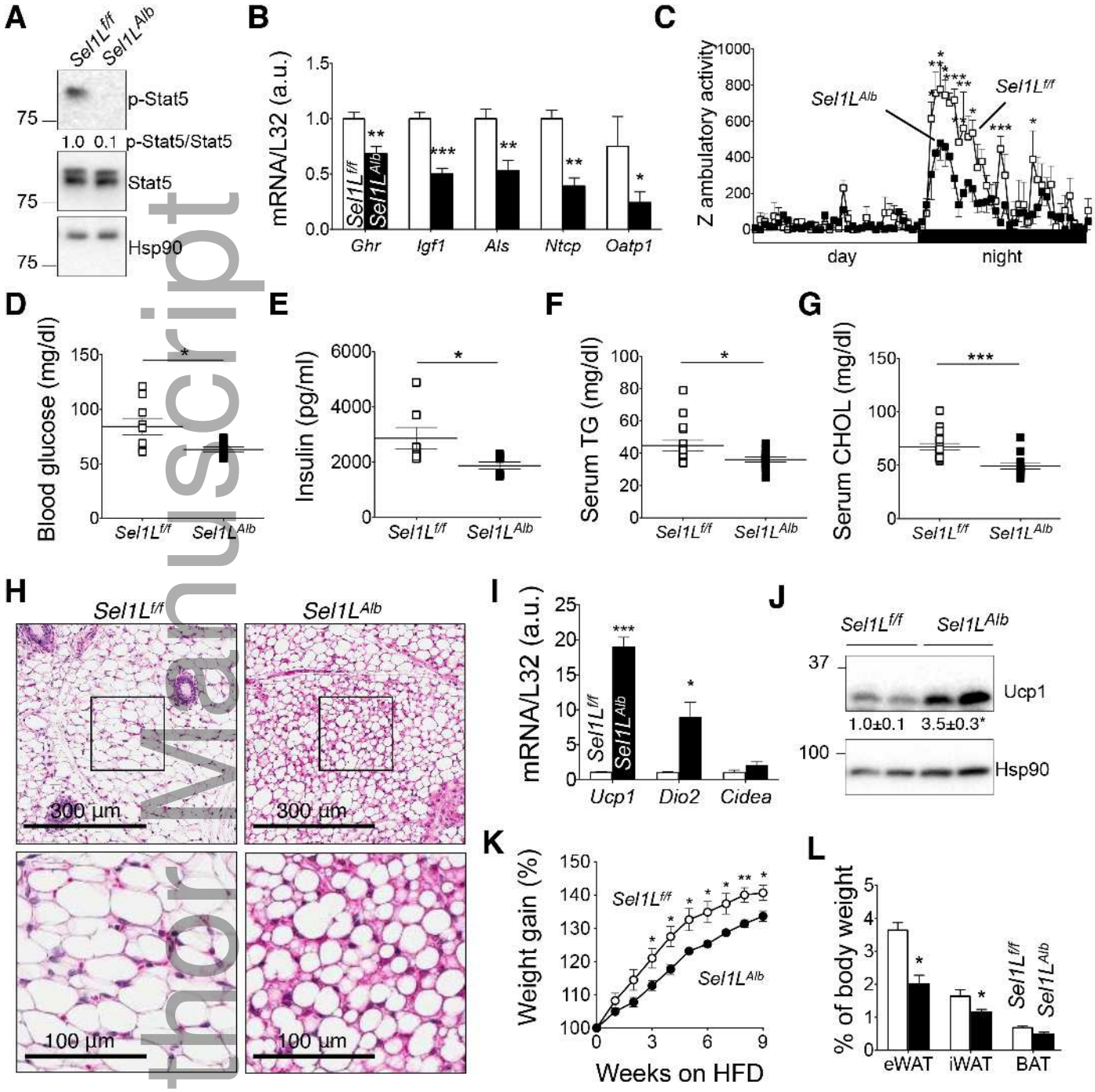


embj_201899277_f3.tif

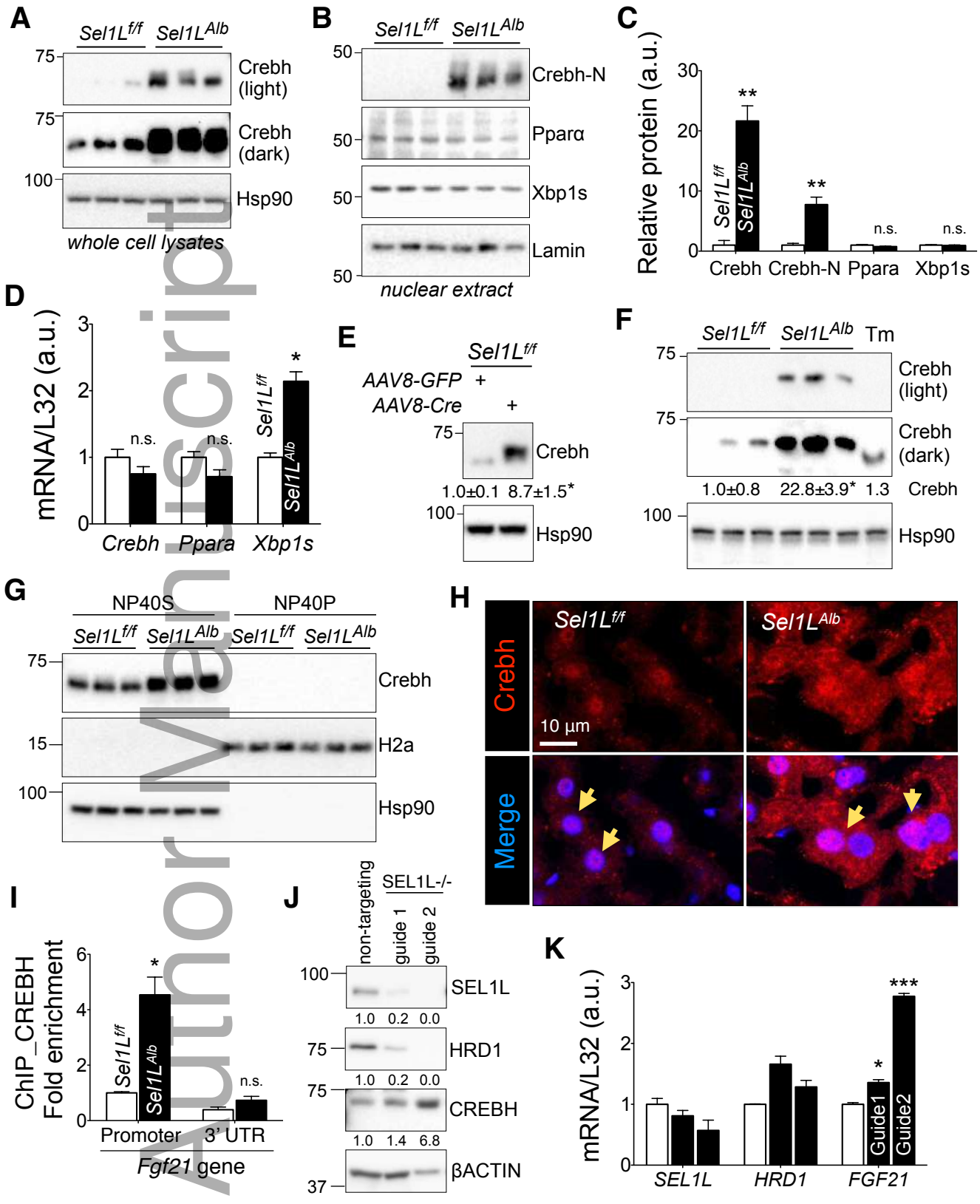

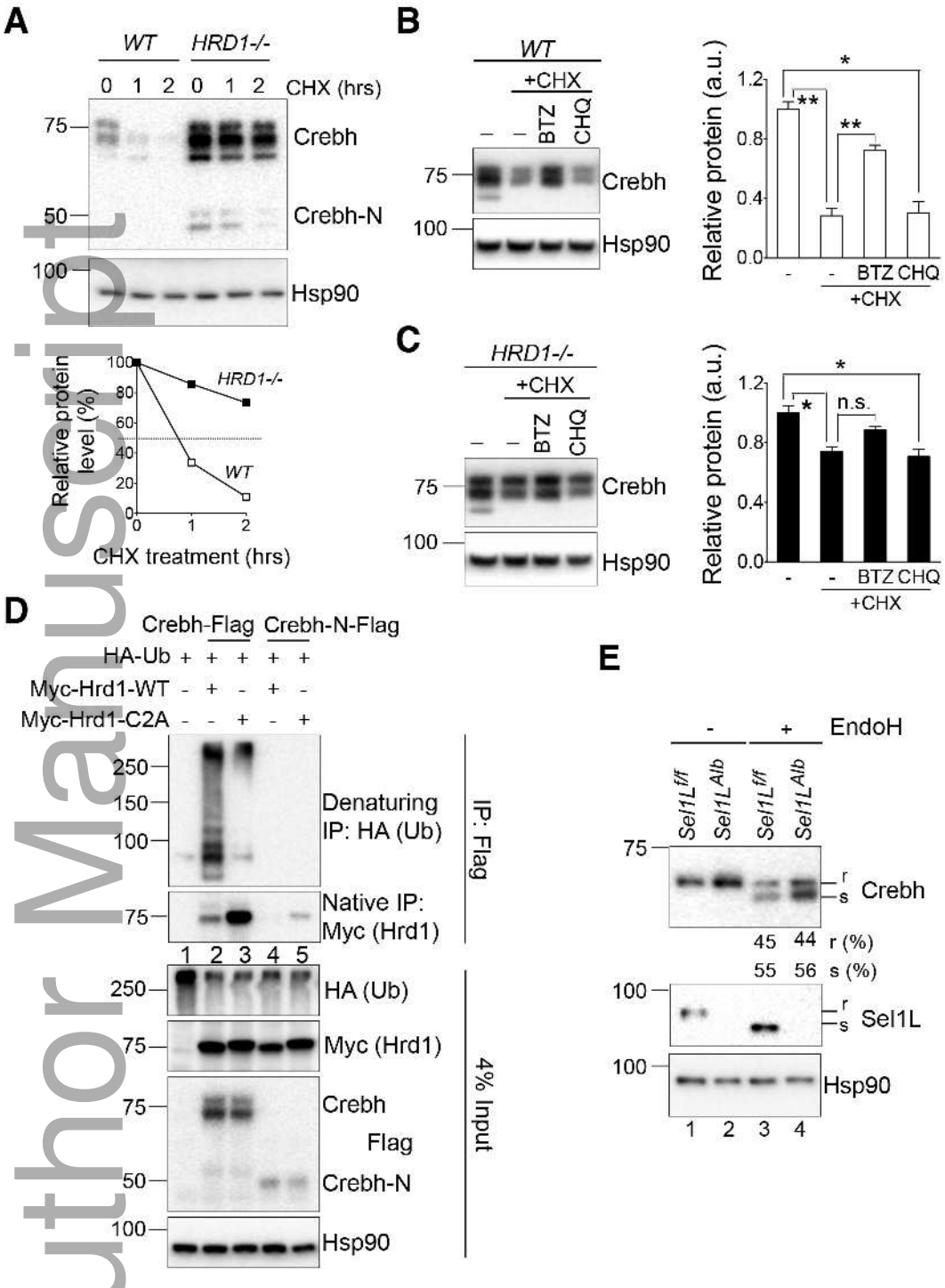


embj_201899277_f5.tif

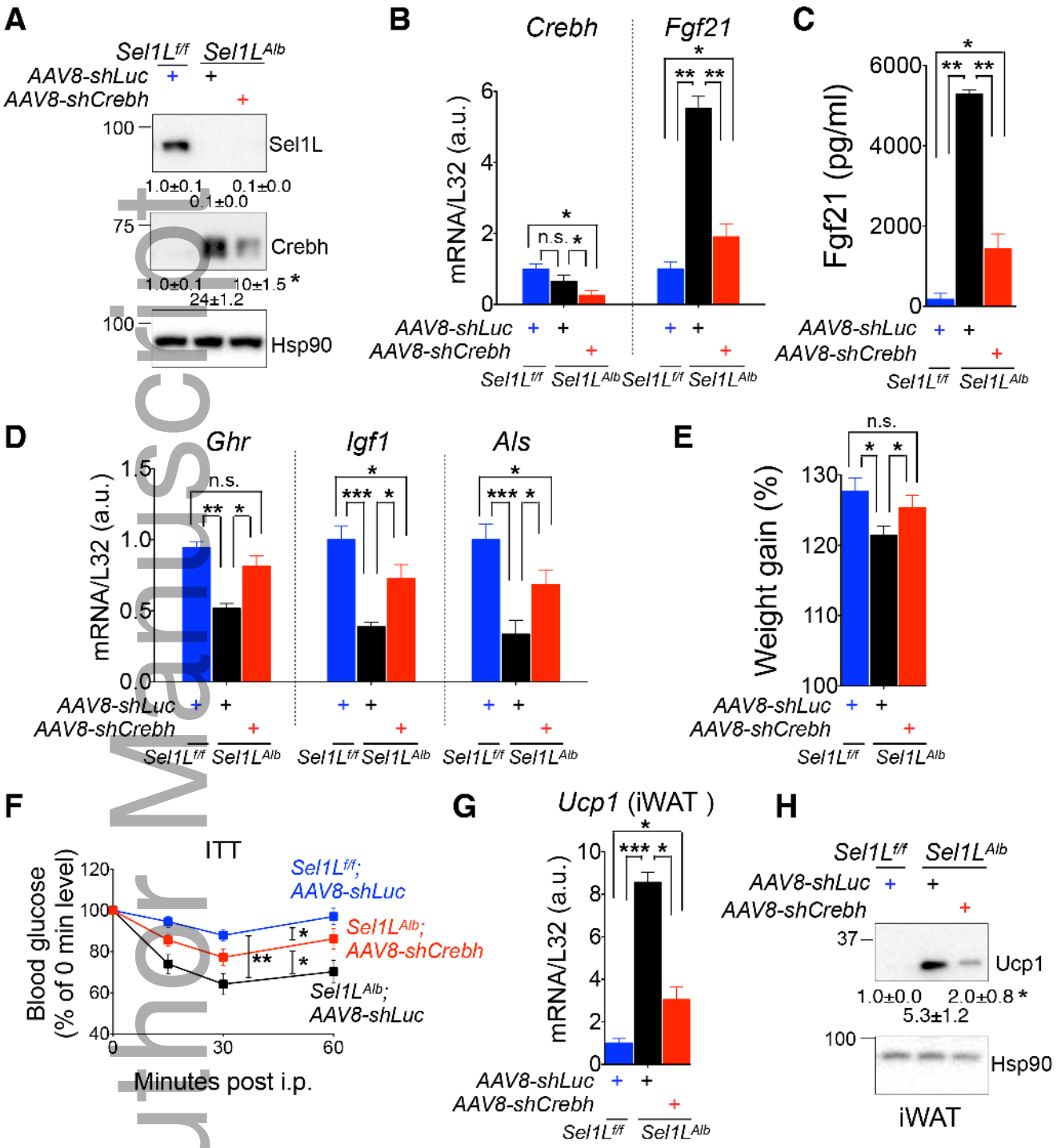


embj_201899277_f6.tif

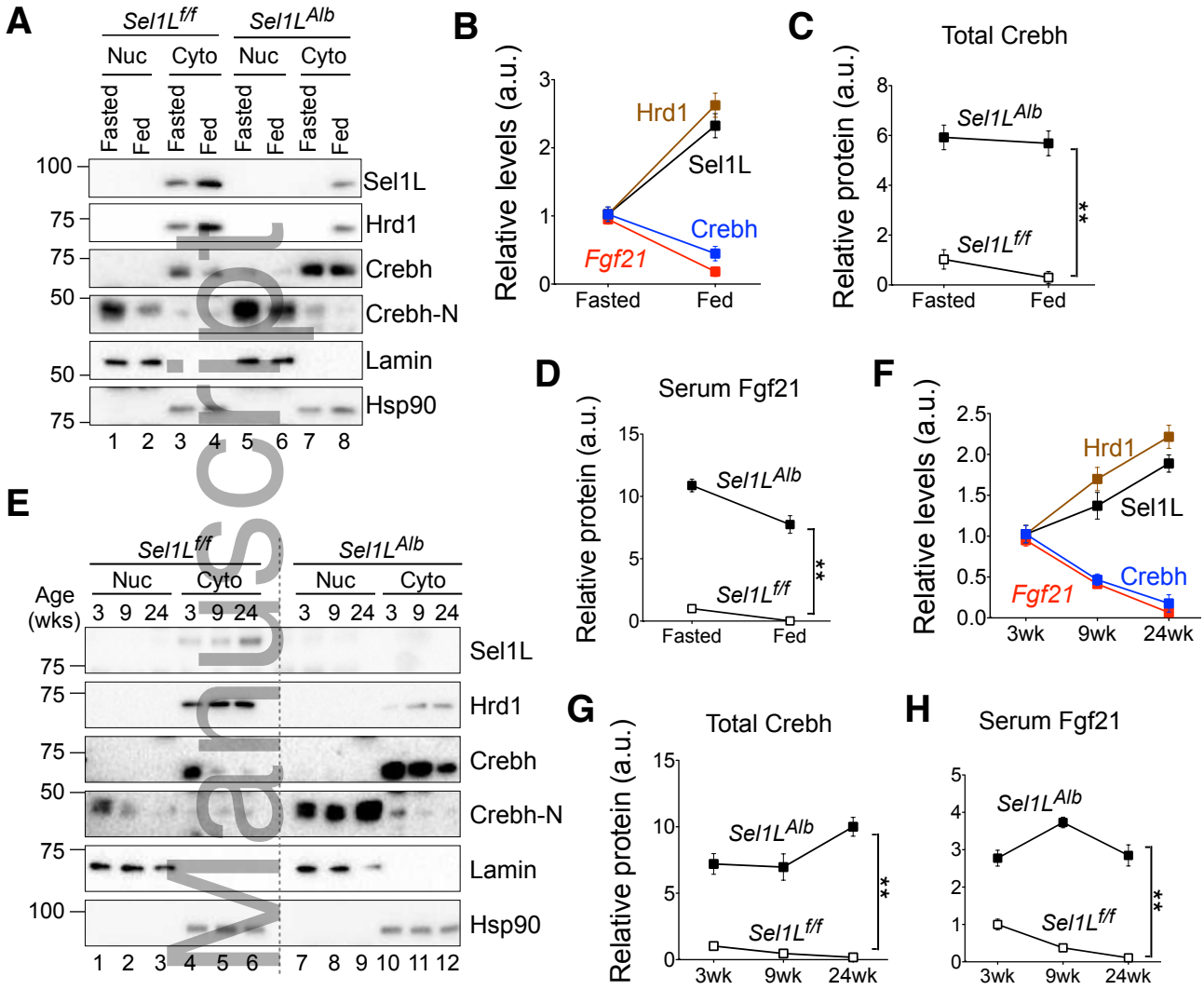

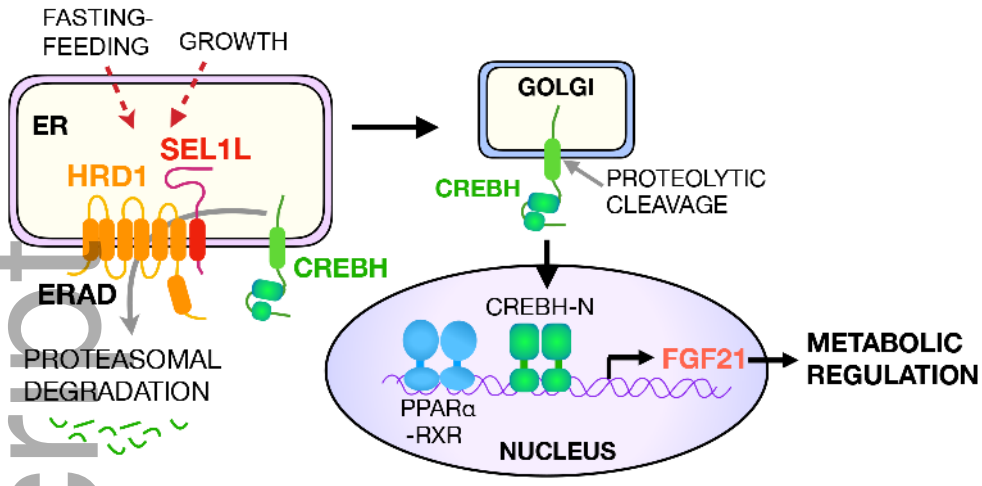


embj_201899277_f8.tif